Fraunhofer Institut
Techno- und
Wirtschaftsmathematik

R. Ciegis, O. Iliev, S. Rief, K. Steiner

On Modelling and Simulation of Different Regimes for Liquid Polymer Moulding

Berichte des Fraunhofer ITWM, Nr. 63 (2004)

ISSN 1434-9973

Bericht 63 (2004)

Die Veröffentlichungen in der Berichtsreihe des Fraunhofer ITWM können bezogen werden über:

Fraunhofer-Institut für Techno- und
Wirtschaftsmathematik ITWM
Gottlieb-Daimler-Straße, Geb. 49

67663 Kaiserslautern
Germany

Telefon: +49 (0) 6 31/2 05-32 42
Telefax: +49 (0) 6 31/2 05-41 39
E-Mail: info@itwm.fraunhofer.de
Internet: www.itwm.fraunhofer.de

Vorwort

Das Tätigkeitsfeld des Fraunhofer Instituts für Techno- und Wirtschaftsmathematik ITWM umfasst anwendungsnahe Grundlagenforschung, angewandte Forschung sowie Beratung und kundenspezifische Lösungen auf allen Gebieten, die für Techno- und Wirtschaftsmathematik bedeutsam sind.

In der Reihe »Berichte des Fraunhofer ITWM« soll die Arbeit des Instituts kontinuierlich einer interessierten Öffentlichkeit in Industrie, Wirtschaft und Wissenschaft vorgestellt werden. Durch die enge Verzahnung mit dem Fachbereich Mathematik der Universität Kaiserslautern sowie durch zahlreiche Kooperationen mit internationalen Institutionen und Hochschulen in den Bereichen Ausbildung und Forschung ist ein großes Potenzial für Forschungsberichte vorhanden. In die Berichtreihe sollen sowohl hervorragende Diplom- und Projektarbeiten und Dissertationen als auch Forschungsberichte der Institutsmitarbeiter und Institutsgäste zu aktuellen Fragen der Techno- und Wirtschaftsmathematik aufgenommen werden.

Darüberhinaus bietet die Reihe ein Forum für die Berichterstattung über die zahlreichen Kooperationsprojekte des Instituts mit Partnern aus Industrie und Wirtschaft.

Berichterstattung heißt hier Dokumentation darüber, wie aktuelle Ergebnisse aus mathematischer Forschungs- und Entwicklungsarbeit in industrielle Anwendungen und Softwareprodukte transferiert werden, und wie umgekehrt Probleme der Praxis neue interessante mathematische Fragestellungen generieren.

Prof. Dr. Dieter Prätzel-Wolters
Institutsleiter

Kaiserslautern, im Juni 2001

On Modelling and Simulation of different Regimes for Liquid Polymer Moulding

R. Čiegis, O. Iliev, S. Rief, K. Steiner

April 28, 2004

Abstract

In this paper we consider numerical algorithms for solving a system of nonlinear PDEs arising in modeling of liquid polymer injection. We investigate the particular case when a porous preform is located within the mould, so that the liquid polymer flows through a porous medium during the filling stage. The nonlinearity of the governing system of PDEs is due to the non-Newtonian behavior of the polymer, as well as due to the moving free boundary. The latter is related to the penetration front and a Stefan type problem is formulated to account for it. A finite-volume method is used to approximate the given differential problem. Results of numerical experiments are presented.

We also solve an inverse problem and present algorithms for the determination of the absolute preform permeability coefficient in the case when the velocity of the penetration front is known from measurements.

In both cases (direct and inverse problems) we emphasize on the specifics related to the non-Newtonian behavior of the polymer. For completeness, we discuss also the Newtonian case. Results of some experimental measurements are presented and discussed.

Keywords: *Liquid Polymer Moulding, Modelling, Simulation. Infiltration, Front Propagation, non-Newtonian flow in porous media*

1 Introduction

Composite materials are widely used in automotive, aerospace, railroad, marine and many other industries. Liquid composite moulding is a family of technologies to manufacture composite materials. These technologies (see, e.g., [5, 35, 38, 43]) are of strong economical interest for manufacturing high quality composite parts. The essence of the discussed technologies is that

a dry fibrous mat, which forms a porous preform, is located within the mould, and after that the liquid polymer is injected. In this way an accurate orientation of the fibers within the composite parts is achieved, making moulding parts with desired mechanical properties. In order to reduce the production costs of manufactured parts, mathematical modeling and numerical simulation are more and more extensively used at the designing stage. Since the filling of the mould is the most critical part of the process, most of the effort is concentrated on its study. The review articles [9, 39] give an impression about most of the mathematical models and numerical algorithms developed in this area. The great part of the models (see, e.g., [9] and references therein) use the linear Darcy model to describe the liquid polymer flow through the porous preform, the latter being considered in rigid body approximation. It should be noted, that such models are not valid for the flow of non-Newtonian fluids. Moreover, they do not account for the compressibility of the fibrous mat and, therefore, these models have a limited range of applicability in modeling polymer moulding. More advanced models consider either the coupled problem for Newtonian fluids in deformable porous media (see, e.g., [1, 18, 19, 20, 21, 39]), or the flow of a non-Newtonian fluid in a rigid porous medium (see, e.g., [44]). The most complete formulation concerning non-Newtonian flow in deformable porous medium is still not well studied.

Several challenging mathematical problems have to be solved in connection with simulation of liquid polymer moulding. Among them are developing of accurate numerical algorithms for solving the nonlinear free boundary direct problems, analysing and solving inverse problems (e.g., parameter estimation, etc.). This paper concerns several aspects of the modeling of LPM processes. These are:

(i) presenting a complete model for flow of non-Newtonian fluids in deformable porous media;

(ii) solving an inverse problem for determining permeability in the case when the penetration front is known from the measurements;

(iii) developing a finite volume algorithm for solving the 1-D direct problem.

First of all, a complete model for flow of non-Newtonian fluids in deformable porous media is listed. Curing (i.e., polymerization) is also accounted for. The model assumes a sharp interface between the filled (wet) part of the porous preform and the unfilled (dry) part. A justification of this assumption for certain process regimes can be found, e.g., in [39]. For the approach dealing with an unsaturated subregion we refer to the discussion

in [9]. In the next section we recall the 3-D model from [18, 19, 20, 21, 39] which treats Newtonian fluids, but accounts for the deformation of the preform and for the curing. The third section is devoted to a more detailed discussion of the model for the 1-D case. The fourth section concerns an extension of this model to the case of the non-Newtonian fluids.

Parameter (i.e., permeability) identification is discussed in Section 3 in the Newtonian case and in Section 4 in the non-Newtonian case. In Section 5 the Forchheimer law is formulated instead of Darcy's law for large flow velocities, when inertial effects become important.

The evaluation of the permeability of a porous material is a very important step in optimization of liquid composite moulding technologies. Currently, the most reliable method for the determination of the permeability is experimental [35]. But it is well known that this approach inherits several major drawbacks (see, [3]). Therefore, a lot of efforts are focused on alternative ways for the evaluation of permeability. The investigations are done on *micro-* and *macro*–scales. For simple preform structures, i.e. unidirectional fiber arrays, random mats, or simplistic fabric–like structures, the results of permeability modeling on the micro–scale are presented in [12, 22, 37, 41]. Simulation on macroscale leads to solving systems of PDE describing the flow of liquid in the porous media, and here some general assumptions on the dependence of the flow velocity on the permeability are usually done a-priori. We should mention that in all experiments the macro–scale behaviour of the flow is observed, thus the interpretation and comparison of the results obtained using a numerical approach are much simpler for macro-scale models. We also mention a paper of Ghaddar [15], where a parallel computational approach for the evaluation of the permeability of unidirectional fibrous media is presented.

The determination of the permeability is critical for the simulation of the filling. Once the permeability is known, the polymer injection can be simulated by analytical or numerical methods. Analytical solutions for the infiltration front position are presented in Section 6 for both cases: Newtonian and non-Newtonian fluids. This information is related to the task of evaluation of permeability and determination of fluid properties.

Section 7 is devoted to a numerical algorithm for solving the governing system of PDEs. Finite volume discretization, treating the moving boundaries, decoupling of the system and results from some numerical experiments, are consecutively discussed there. An algorithm in Lagrangian coordinate system is presented in Section 8. In the last section the results of numerical simulations are presented and discussed.

Some preliminary results of this report were published in [10].

2 Mathematical Model

In this section we introduce the basic equations describing the injection moulding processes. Consider a *deformable* porous medium that at time $t = 0$ starts being infiltrated. Let us denote by D^w and D^d the time-varying domains corresponding to the wet part of the solid preform (i.e., which is already wet by the infiltrating resin), and to the dry one (i.e., which is not yet reached by the liquid polymer), respectively.

We assume that *capillary phenomena* can be neglected, thus D^w and D^d are divided by a sharp interface σ^i that represents the infiltration front. We also neglect the *gravity* force. Both assumptions are reasonable when the applied external pressure is relatively high. Let us denote by σ^e the contact surface between the pure liquid and the wet solid.

The mathematical model consists of evolution equations for the *state variables* in the wet and in the dry regions, completed by interfaces conditions on σ^i and σ^e and by proper boundary conditions. Note that the general multi-component mixture equations can be simplified [20] for the considered case.

2.1 Mathematical Model in the Wet Region

The following variables are used to describe processes in the wet region:

Φ_s^w and Φ_l^w are the volume fraction occupied by the solid and the liquid constituents, respectively. Assuming full saturation, the volume fraction occupied by the liquid satisfies

$$\Phi_l^w = 1 - \Phi_s^w \, .$$

$\mathbf{v}_s^w, \mathbf{v}_l^w$ denote the velocities of the solid and the liquid constituents. P_l^w is the pore liquid pressure. θ^w is the temperature of the mixture in the wet region. Here we assume that the solid and liquid constituents there are locally in thermal equilibrium. δ is the degree of cure of the resin.

Additionally, the model takes into account the fact that during the penetration the liquid undergoes a polymerization process (i.e., *curing*), which is largely exothermic. The degree of cure δ represents the fraction of cured resin. So $0 \leq \delta \leq 1$ (no curing for $\delta = 0$, complete curing for $\delta = 1$).

2.1.1 Mass Conservation of Solid and Liquid Constituents

Assuming that the solid and liquid are incompressible (i.e., the densities of the solid ρ_s and liquid ρ_l are constant), we obtain the local mass conservation equations in the Eulerian framework:

$$\frac{\partial \Phi_s^w}{\partial t} + \nabla \cdot (\Phi_s^w \mathbf{v}_s^w) = 0\,, \tag{1}$$

$$\frac{\partial \Phi_l^w}{\partial t} + \nabla \cdot (\Phi_l^w \mathbf{v}_l^w) = 0\,. \tag{2}$$

Assuming saturation the volume fraction occupied by the liquid is given by

$$\Phi_l^w = 1 - \Phi_s^w\,. \tag{3}$$

Summing up Eqs. (1) and (2) and introducing the *composite velocity* (or *volume average* velocity)

$$\mathbf{v}_c^w = \Phi_s^w \mathbf{v}_s^w + \Phi_l^w \mathbf{v}_l^w\,,$$

and recalling the saturation condition (3) results in the equation

$$\nabla \cdot \mathbf{v}_c^w = 0\,. \tag{4}$$

Let us denote by ρ_m^w the density of the mixture as a whole, i.e.:

$$\rho_m^w = \rho_s \Phi_s^w + \rho_l \Phi_l^w$$

and by $\mathbf{v}_m^w$ the *mass average* velocity of the mixture

$$\mathbf{v}_m^w = \frac{\rho_s \Phi_s^w \mathbf{v}_s^w + \rho_l \Phi_l^w \mathbf{v}_l^w}{\rho_m^w}\,.$$

Summing up Eqs. (1) and (2) multiplied by the corresponding densities gives the following mass conservation equation

$$\frac{\partial \rho_m^w}{\partial t} + \nabla \cdot (\rho_m^w \mathbf{v}_m^w) = 0\,.$$

2.1.2 Momentum Balance Equations

We will not consider the general momentum balance equations. To focus on flow in porous media, the following simplifying assumptions are used [20]:

(A1) Negligible surface tension and capillary effects and slow liquid flow in the porous medium;

(A2) Negligible liquid excess-stress; excess interaction force between the solid and the liquid is proportional to the velocity difference $\mathbf{v}_l^w - \mathbf{v}_s^w$;

(A3) Negligible inertia if compared to the stresses; external body forces (e.g. gravity) are neglected;

Then we write the general momentum balance equations as

$$\Phi_l^w(\mathbf{v}_l^w - \mathbf{v}_s^w) = -\frac{\mathbf{K}}{\mu}\nabla P_l^w\,, \tag{5}$$

$$\nabla P_l^w - \nabla \cdot \mathbf{T}_m^w = 0\,, \tag{6}$$

where μ is the liquid viscosity, which depends on the degree of cure δ and on the temperature θ^w, i.e.

$$\mu = \mu(\theta^w, \delta)\,.$$

The viscosity decreases with increasing temperature and increases with increasing degree of cure. Models used for the description of the viscosity are the following:

$$\mu(\theta,\delta) = \bar{\mu}\exp\big(\frac{A}{\theta}\big)\left(\frac{\delta_g}{\delta_g-\delta}\right)^{c+d\delta}, \quad \mu(\theta,\delta) = \bar{\mu}\exp\big(\frac{A}{\theta}+c\delta\big)\,.$$

$\mathbf{K}$ is the *permeability* tensor, which for saturated deformable porous media depends on the deformation gradient $\mathbf{F}_s$ of the solid constituent $\mathbf{K} = \mathbf{K}(\mathbf{F}_s)$. P_l^w is the pore liquid pressure and $\mathbf{T}_m^w$ is the effective stress tensor.

Equation (5) is known as *Darcy's law* for deformable porous media. Here the effects of gravity are neglected, since normally for resin injection processes the pressure gradient is large compared to the value of the gravitation term. A critical discussion of the hypotheses underlying Darcy's law is given in [32, 34]. Several generalizations of Darcy's law can be used here, e.g. Forchheimer law to account for fast flows, or correction to take into account the non-Newtonian properties of the resin. Both generalizations are discussed in the next sections.

To complete the model, one has to specify the constitutive equation for the stress tensor $\mathbf{T}_m^w$. We will present such equations later for the one–dimensional case of the model.

2.1.3 Energy Balance

Following the same procedure, which was used in previous sections, it is possible to write the energy equation for the mixture:

$$\rho_m c_m \left(\frac{\partial \theta^w}{\partial t} + \mathbf{v}_m^w \cdot \nabla \theta^w \right) = \nabla \cdot (\mathbf{\Lambda}_m^w \nabla \theta^w) + \frac{1}{\mu} \mathbf{K} \nabla P^w \cdot \nabla P^w \qquad (7)$$
$$+ \Phi_l^w H_c f_c(\delta, \theta^w) - \frac{\rho_s \rho_l \Phi_s^w \Phi_l^w}{\rho_m} (c_l - c_s)(\mathbf{v}_l^w - \mathbf{v}_s^w) \cdot \nabla \theta^w \,,$$

where c_m is the specific heat of the mixture:

$$c_m = \frac{\rho_s \Phi_s^w c_s + \rho_l \Phi_l^w c_l}{\rho_m} \,.$$

$\mathbf{\Lambda}_m^w$ is the thermal conductivity tensor of the entire mixture, the term $\Phi_l^w H_c f_c(\delta, \theta^w)$ represents the heat generated by the curing reaction of the resin and the last term represents the heat diffusion due to the relative motion.

2.1.4 The Degree of Curing

As the liquid is moving, the evolution of the degree of cure is modeled by the equation

$$\frac{\partial \delta}{\partial t} + \mathbf{v}_l^w \cdot \nabla \delta = f_c(\delta, \theta^w) \,, \qquad (8)$$

where f_c is an experimentally determined function describing the chemical reaction. The most popular model is proposed by Kamal–Sorour:

$$f_c(\delta, \theta) = (K_1 + K_2 \delta^m)(1 - \delta)^n, \quad K_i = c_i exp\left(-\frac{E_i}{R\theta} \right) \,,$$

where R is the universal gas constant, E_i are the activation energies and c_i are the characteristic constants for the reactions.

2.2 Mathematical Model in the Dry Region

We proceed in a way similar to the one outlined for the wet region. However, some additional assumptions are used, which enable us to simplify the model.

(D1) The air pressure is everywhere equal to the atmospheric pressure;

(D2) The gas contribution to the global stress may be neglected;

(D3) The mass average velocity is equal to the velocity of the solid constituent and the composite density $\rho_m \approx \Phi_s^d \rho_s$, but the composite velocity

$$\mathbf{v}_c = \Phi_s \mathbf{v}_s + (1 - \Phi_s)\mathbf{v}_{air} \,.$$

Thus, we have the following state variables in the dry region: Φ_s^d is the solid volume fraction, $\mathbf{v}_s^d$ is the solid velocity and θ^d is the temperature.

Mass Conservation The equation of mass conservation reads

$$\frac{\partial \Phi_s^d}{\partial t} + \nabla \cdot (\Phi_s^d \mathbf{v}_s^d) = 0 \,. \tag{9}$$

Momentum Balance Equation The deformation of the dry solid part is governed by the momentum balance equation

$$\nabla \cdot \mathbf{T}_s^d = 0 \,, \tag{10}$$

where $\mathbf{T}_s^d$ is the stress tensor of the dry medium. Here we assume, that $\mathbf{T}_m^d = \mathbf{T}_s^d$.

As mentioned above, in order to complete the model we still have to specify the constitutive equations for the stress tensors $\mathbf{T}_m^w$ and $\mathbf{T}_s^d$. We assume that the wet and dry solids behave *elastically*.

Energy Balance Equation The Energy balance equation reads

$$\rho_s \Phi_s^d c_s \left(\frac{\partial \theta^d}{\partial t} + \mathbf{v}_s^d \cdot \nabla \theta^d \right) = \nabla \cdot \left(\Phi_s^d \mathbf{\Lambda}_s^w \nabla \theta^d \right) \,, \tag{11}$$

where $\mathbf{\Lambda}_s^w$ is the thermal conductivity of the solid.

2.3 Interface and Boundary Conditions

Infiltration Front

Let the infiltration interface σ^i be given by the surface

$$\psi_i(x, y, z, t) = 0 \,.$$

This surface moves together with the propagation of the liquid, thus its evolution equation is given by

$$\frac{\partial \psi_i}{\partial t} + \mathbf{v}_l^w(\sigma^i) \cdot \nabla \psi_i = 0 \,. \tag{12}$$

Preform Border

Let the contact surface σ^e between the liquid and the wet solid be given by

$$\psi_e(x, y, z, t) = 0\,.$$

As the resin penetrates the porous solid this material surface is fixed on the solid, and therefore its evolution equation is

$$\frac{\partial \psi_e}{\partial t} + \mathbf{v}_s^w(\sigma^e) \cdot \nabla \psi_e = 0\,. \tag{13}$$

Jump Conditions for Material Surfaces

Considering the mixture as a whole, the following jump conditions are obtained for material surfaces [18, 20, 31]

$$[\rho_m(\mathbf{v}_m - \mathbf{v}_\sigma)] \cdot \mathbf{n}_\sigma = 0\,, \tag{14}$$
$$[\theta] = 0\,, \tag{15}$$
$$[-P_l\,\mathbf{I} + \mathbf{T}_m] \cdot \mathbf{n}_\sigma = 0\,, \tag{16}$$
$$[P_l] = 0\,, \tag{17}$$

where $\mathbf{n}_\sigma$ is the normal outside D^w. It follows from (14) that

$$[\mathbf{v}_c] \cdot \mathbf{n}_\sigma = 0\,.$$

Using (16), (17) gives the continuity of the stress $\mathbf{T}_m$ across the the surface:

$$[\mathbf{T}_m] \cdot \mathbf{n}_\sigma = 0\,.$$

In the one-dimensional case assuming the same constitutive equation of elastic type for wet and dry solids, this implies the continuity of Φ_s across σ^i, and then we get from (14) the continuity of $\mathbf{v}_s$.

If the specific heat of the solid is continuous across σ^i, the temperature fluxes satisfy the following condition:

$$[\mathbf{\Lambda}_m \nabla \theta] \cdot \mathbf{n}_\sigma = 0\,.$$

Boundary Conditions on σ^e

Let the superscript $^-$ denotes the quantities evaluated in the pure liquid region. Then we have the following conditions

$$\Phi_s^- = 0, \quad \mathbf{v}_l^- = \mathbf{v}_{in}\,,$$
$$\mathbf{T}_m^-\,\mathbf{n}_{\sigma^e} = 0, \quad P_l^- = P_0\,,$$

where $\mathbf{v}_{in}$ is the inflow velocity of the resin and P_0 the pressure driving the flow. Thus, in the wet region we have $\Phi_s^w(\sigma^e, t) = \Phi_r$, where Φ_r is the solid volume fraction in the dry undeformed preform.

The temperature on σ^e is $\theta = \theta_{in}$, where θ_{in} is the temperature of the infiltrating liquid.

Boundary Conditions for the Curing Equation

The curing equation (8) is hyperbolic. Hence, the boundary conditions

$$\delta(\sigma^e) = \delta_{in}$$

must be specified on the part of the boundary where the characteristics enter the domain (the resin enters the preform), i.e. where $(\mathbf{v}_l^w - \mathbf{v}_s^w) \cdot \mathbf{n}_{\sigma^e} < 0$.

3 One-Dimensional Infiltration

This section deals with one-dimensional problems (see [1, 18, 20, 21]). Unidirectional injection is obtained in a flat mold of constant thickness when one side of the mold is connected to an injection channel. It is assumed that the permeability is homogenous and boundary effects can be neglected. Then the flow front is a straight line and the 1D model can be used to describe this case.

Assume that the porous medium is initially dry, homogeneous, isotropic and that the flow and the strain take place only along the x axis. Let us denote by $x = x_e(t)$ the left border of the preform, which can move (due to the preform's compression) when the liquid touches it. The infiltration front $x = x_i(t)$ separates the wet region D^w from the remaining dry region D^d:

$$D^w = [x_e(t), x_i(t)], \quad D^d = [x_i(t), L] .$$

As infiltration proceeds, the dry and the wet preforms compress or expand back according to the process conditions.

The one-dimensional mathematical model is obtained from the system of equations given in the previous section.

For $t \leq 0$ the whole preform is dry, at rest, and compressed at a given volume ratio:

$$\begin{cases} \Phi_s^d(x, t = 0) = \Phi_r, \quad x \in [0, L] , \\ x_e(t = 0) = 0, \quad x_i(t = 0) = 0 , \end{cases}$$

where Φ_r is the solid volume fraction of the solid preform in its undeformed configuration.

3.1 Wet Region

In the wet region the following equations are satisfied:

$$\frac{\partial \Phi_s^w}{\partial t} + \frac{\partial}{\partial x}\left(\Phi_s^w v_s^w\right) = 0\,, \tag{18}$$

$$\Phi_s^w(x_e(t),t) = \Phi_r, \;\; t > 0\,,$$

$$\frac{\partial v_c^w}{\partial x} = 0\,, \tag{19}$$

$$(1-\Phi_s^w)(v_l^w - v_s^w) = -\frac{K}{\mu(\delta,\theta^w)}\,\frac{\partial P_l^w}{\partial x}\,, \tag{20}$$

$$\frac{\partial P_l^w}{\partial x} = \frac{\partial \tau^w}{\partial x}\,, \tag{21}$$

$$\rho_m c_m\left(\frac{\partial \theta^w}{\partial t} + v_m^w \frac{\partial \theta^w}{\partial x}\right) = \frac{\partial}{\partial x}\left(\lambda_m \frac{\partial \theta^w}{\partial x}\right) + \frac{\rho_s \rho_l}{\rho_m}(c_l - c_s)\Phi_s^w$$

$$\times \frac{K}{\mu(\delta,\theta^w)}\frac{\partial \tau^w}{\partial x}\frac{\partial \theta^w}{\partial x} + (1-\Phi_s^w)H_c f_c(\delta,\theta^w) + \frac{K}{\mu(\delta,\theta^w)}\left(\frac{\partial \tau^w}{\partial x}\right)^2\,, \tag{22}$$

$$\frac{\partial \delta}{\partial t} + v_l^w \frac{\partial \delta}{\partial x} = f_c(\delta,\theta^w)\,, \tag{23}$$

where τ^w is the xx component of $\mathbf{T}_m$:

$$\tau^w = (\mathbf{T}_m)_{xx}\,, \;\; x \in D^w,\; t \geq 0\,,$$

and K is the xx component of the permeability tensor $K = (\mathbf{K})_{xx}$.

3.1.1 Constitutive Models

We still need to specify the constitutive equations for the stresses. At equilibrium the stress is usually related to the strain by a nonlinear relation, which can be determined by static stress–strain measurements. It should be noted that in one–dimensional problems the strain is related to volume ratio, i.e. to Φ_s.

Two models can be used.

(WA1) The elastic model for the wet porous medium preform reads

$$\tau^w = -\Sigma_w(\Phi_s^w)\,,$$

where Σ_w is a strictly increasing function. Frequently, it is assumed that

$$\Sigma_d = \Sigma_w \,.$$

Then the continuity of the stress across x_i implies also the continuity of the Φ_s. If wet and dry preforms behave elastically with $\Sigma_d \neq \Sigma_w$, the continuity of Φ_s across x_i does not hold any more.

(WA2) Due to the fact that the solid and the liquid matrices can not deform independently but have to carry the load by joint deformations, the wet preform can be modeled using a nonlinear Kelvin–Voigt law:

$$\lambda \left(\frac{\partial \tau^w}{\partial t} + v_s^w \frac{\partial \tau^w}{\partial x} \right) + \tau^w = \Lambda \left(\frac{\partial \Sigma_w(\Phi_s^w)}{\partial t} + v_s^w \frac{\partial \Sigma_w(\Phi_s^w)}{\partial x} \right) + \Sigma_w(\Phi_s^w) \,,$$

where λ is called the relaxation time, Λ is the retardation time, and the following inequality $\Lambda \geq \lambda$ is satisfied. If $\lambda = \Lambda$ and suitable initial conditions are used, then this equation has the solution:

$$\tau^w = -\Sigma_w(\Phi_s^w) \,,$$

i.e. the material behaves elastically.

(DA3) The dry preform is always assumed to behave elastically

$$\tau^d = -\Sigma_d(\Phi_s^d) \,, \tag{24}$$

where Σ_d is a strictly increasing function of the solid volume fraction.

3.1.2 Velocity Driven Infiltration

Before formulating equations in the dry region D^d we will use equation (19), from which it follows that v_c is space independent in D^w

$$v_c(x,t) = v(t) \,.$$

The boundary $x_e(t)$ is fixed to the solid phase and moves with the velocity v_s. Specializing the jump condition formulated in the previous section and writing it for the one–dimensional problem

$$[\rho_m(v_m - v_s)] = 0 \,,$$

one can obtain the following equalities:

$$\rho_m(v_m - v_s) = \rho_l \Phi_l (v_l - v_s) = \rho_l (v_c - v_s) \,.$$

Taking the limits on both sides of the boundary we prove that the composite velocity is continuous across $x_e(t)$, and thus we have:

$$v_c(x,t) = u_{in}(t), \quad x \in D^w \,.$$

Here $u_{in}(t)$ is the velocity of the infiltrated liquid.

Using Darcy's law (20) we can express the velocities of the solid and liquid constituents

$$\begin{aligned} v_s^w &= u_{in} + \frac{K}{\mu}\frac{\partial P_l^w}{\partial x}\,, \\ v_l^w &= u_{in} - \frac{\Phi_s^w}{1-\Phi_s^w}\frac{K}{\mu}\frac{\partial P_l^w}{\partial x}\,. \end{aligned} \tag{25}$$

The infiltration front $x_i(t)$ moves with the liquid, thus we have the initial value problem

$$\begin{cases} \dfrac{dx_i(t)}{dt} = v_l^w(x_i(t),t) = u_{in} + \left(\dfrac{\Phi_s^w}{1-\Phi_s^w}Q\right)(x_i(t),t)\,, \\ x_i(t=0) = 0\,, \end{cases} \tag{26}$$

where Q is given by

$$Q = -\frac{K}{\mu}\frac{\partial P_l^w}{\partial x} = -\frac{K}{\mu}\frac{\partial \tau^w}{\partial x}$$

and evaluated at the infiltration front from the wet region.

Determination of the Permeability

It follows from (25) that the permeability of the homogeneous structure can be determined as

$$K = (u_{in} - v_l^w)\ \frac{(1-\Phi_s^w)\mu}{\Phi_s^w}\ \left(\frac{\partial P_l^w}{\partial x}\right)^{-1}\,,$$

if experimental measurements of the interface velocity $v_l^w(x_i(t),t)$, the volume fraction occupied by the solid Φ_s^w and pressure gradients are available.

3.2 Dry Region

Since the interaction between the air and the solid can be assumed negligible, there is no pressure drop in the air. Therefore $P^d(x,t) = P_{atm}$, where P_{atm} is the atmospheric pressure.

Let τ^d be the xx component of the excess stress tensor in the dry region, then we obtain

$$\frac{\partial \tau^d}{\partial x} = 0\,. \tag{27}$$

If the dry preform is assumed to behave elastically, then equations (24) and (27) imply that Φ_s^d is space independent, i.e.

$$\Phi_s^d = \Phi_s^d(t)\,. \tag{28}$$

Then the continuity equation implies that

$$\frac{\partial \Phi_s^d}{\partial t} + \Phi_s^d(t)\frac{\partial v_s^d}{\partial x} = 0$$

and the velocity satisfies the linear ODE with respect to the space coordinate:

$$\frac{\partial v_s^d}{\partial x} = -\frac{\frac{d}{dt}(\Phi_s^d(t))}{\Phi_s^d(t)}\,. \tag{29}$$

Integrating equation (29) over the interval $[x_i, L]$ and using the boundary condition

$$v_s^d(L,t) = 0\,,$$

(i.e. the preform is constrained by a fixed draining boundary at $x = L$ and its velocity vanishes there), one has

$$v_s^d(x,t) = \frac{\frac{d}{dt}(\Phi_s^d(t))}{\Phi_s^d}(L-x)\,.$$

Neglecting the influence of the air, we get the simplified heat equation

$$\rho_s c_s \left(\Phi_s^d \frac{\partial \theta^d}{\partial t} + \frac{d\Phi_s^d}{dt}(L-x)\frac{\partial \theta^d}{\partial x}\right) = \frac{\partial}{\partial x}\left(\Phi_s^d \lambda_s \frac{\partial \theta^d}{\partial x}\right)\,. \tag{30}$$

3.2.1 Velocity Driven Infiltration

Now we will finish the analysis of this case. ¿From the general jump conditions formulated in the previous section (here we use the velocity of the infiltration interface) one can obtain the following equalities:

$$\rho_m(v_m - v_l) = \rho_s \Phi_s (v_s - v_l) = \rho_s (v_c - v_l)\,.$$

Then after simple computations it follows that v_c is also continuous across the interface $x_i(t)$

$$v_c^w(x_i(t),t) = v_c^d(x_i(t),t)\,,$$

thus it is equal to the inflow velocity

$$v_c(x,t) = u_{in}(t), \quad x \in D^d\,.$$

The continuity of v_c across the infiltration front and the fact that $x_i(t)$ is a material interface fixed on the liquid phase

$$\frac{dx_i(t)}{dt} = v_l(x_i(t),t)$$

leads to the initial value problem

$$\begin{cases} \dfrac{d}{dt}\Big(\big(1-\Phi_s^d(t)\big)\big(L-x_i(t)\big)\Big) = -u_{in}(t)\,, \\ \Phi_s^d(0) = \Phi_{s0}^d\,. \end{cases} \tag{31}$$

The solution of (31) can be obtained in the explicit form:

$$\Phi_s^d(t) = \frac{1}{L-x_i(t)}\left(\int_0^t u_{in}(s)\,ds - x_i(t) + L\Phi_{s0}^d\right)\,. \tag{32}$$

This equation should be solved with the initial value problem (26), which specifies the development of the infiltration front $x_i(t)$.

3.2.2 Pressure Driven Infiltration

If the inlet pressure $\Delta P(t) = P_0(t) - P_{atm}$ is given, then we can integrate the momentum equation (21) and use the continuity of the stress on the infiltration front:

$$\tau^d(t) = \Delta P(t), \;\; t > 0\,.$$

Then the solid volume fraction of the dry region is given as

$$\Phi_s^d(t) = \Sigma_d^{-1}\big(\Delta P(t)\big)\,.$$

Using this formula and the mass conservation we can find the initial position of the left border of the preform after incoming liquid compresses the preform:

$$x_e(0) = L\left(1 - \frac{\Phi_r}{\Phi_s^d(0)}\right)\,.$$

Taking the equation (31) and using (25) to eliminate u_{in} from the obtained equation gives the initial value problem for the interface $x_i(t)$:

$$\begin{cases} \dfrac{d(\Phi_s^d x_i)}{dt} = L\dfrac{d\Phi_s^d}{dt} + \left(\dfrac{\Phi_s^w Q}{1-\Phi_s^w}\right)(x_i(t),t)\,, \\ x_i(0) = x_{i0}\,. \end{cases} \tag{33}$$

The inflow velocity is then determined as

$$\begin{aligned} u_{in}(t) &= \Phi_s^d v_s + (1-\Phi_s^d)v_l \\ &= \big(L - x_i(t)\big)\frac{d\Phi_s^d(t)}{dt} + \big(1-\Phi_s^d\big)\frac{dx_i(t)}{dt}\,. \end{aligned} \tag{34}$$

If $\Delta P(t)$ is constant in time, one obtains:

$$u_{in}(t) = (1-\Phi_s^d)\,\frac{dx_i(t)}{dt}\,.$$

4 Non-Newtonian Flow

In the previous section we considered Newtonian fluids, for which Darcy's law specifies the relation between the velocity and the pressure. But a large number of fluids, such as polymer solutions, polymer melts, suspensions do not follow Newton's law of viscosity [16]. The flow of polymer resin through fibrous materials is a very important process in the resin transfer moulding technology. The literature on non–Newtonian fluid flows is far less complete (see an overview in [45]). Some experimental results are presented in [44], a numerical study is given in [48].

One of the possibilities to describe non-Newtonian fluids is to modify the classical Darcy's law and to use a generalized Darcy's law (*power law*). For the one-dimensional case we have:

$$(1-\Phi_s^w)(v_l^w - v_s^w) = \left(-\frac{K}{H}\,\frac{\partial P_l^w}{\partial x}\right)^{1/n}\,, \tag{35}$$

where n is used to describe different types of fluids. If $n<1$ then a fluid is *pseudoplastic* (polymer solutions are pseudoplastic). *Dilatant* fluids are described using $n>1$. Here H is the non-Newtonian bed factor. Following [8] we combine a power law model of a non-Newtonian fluid with the Blake-Kozeny model for the porous medium. We obtain

$$H = \frac{\mu}{12}\left(9+\frac{3}{n}\right)^n (150K\epsilon)^{(1-n)/2}\,,$$

where ϵ is the porosity of the structure. Then equation (35) can be rewritten as:

$$(1-\Phi_s^w)(v_l^w - v_s^w) = \left(-\frac{K^{(1+n)/2}}{\mu\ d_n}\ \frac{\partial P_l^w}{\partial x} \right)^{1/n}, \tag{36}$$

$$d_n = \frac{1}{12}\left(9+\frac{3}{n}\right)^n (150\epsilon)^{(1-n)/2}.$$

Determination of the Permeability

Using the generalized Darcy's law (36) and the fact that v_c is constant in space we can express the velocity of the liquid constituent

$$v_l^w = u_{in} + \frac{\Phi_s^w}{1-\Phi_s^w}\left(-\frac{K^{(1+n)/2}}{\mu\ d_n}\frac{\partial P_l^w}{\partial x} \right)^{1/n}. \tag{37}$$

The infiltration front $x_i(t)$ moves with the liquid, thus we have the initial value problem

$$\begin{cases} \dfrac{dx_i(t)}{dt} = v_l^w(x_i(t),t) = u_{in} + \dfrac{\Phi_s^w}{1-\Phi_s^w}\left(-\dfrac{K^{(1+n)/2}}{\mu\ d_n}\dfrac{\partial P_l^w}{\partial x} \right)^{1/n}, \\ x_i(t=0) = 0\,. \end{cases}$$

After measuring the front velocity $v_l^w(x_i(t),t)$, the volume fraction corresponding to the solid Φ_s^w and the pressure gradient we can determine the permeability of the homogeneous structure as

$$K = \left(-\left((v_l^w - u_{in})\ \frac{1-\Phi_s^w}{\Phi_s^w} \right)^n \mu\, d_n \left(\frac{\partial P_l^w}{\partial x} \right)^{-1} \right)^{2/(1+n)}.$$

5 The Forchheimer law

Darcy's law states the linearity between velocity and pressure. It holds for slow flows when the inertial effects of the flow are negligible. In this section we consider one more correction to Darcy's law for large enough flow speed. Then the relation between the velocity and the pressure is nonlinear. The following equation has been proposed by Forchheimer and

investigated by many authors (see, e.g. [2, 26, 29, 40]). We consider only the *one–dimensional* case of the equation

$$\frac{\mu}{K}u + \frac{\rho_l c_F}{K^{1/2}}\,|u|\,u = -\frac{\partial P_l^w}{\partial x}\,, \tag{38}$$

where $u = \Phi_l^w(v_l^w - v_s^w)$ and c_F is the Forchheimer or inertia coefficient. Eq. (38) is the two phase flow Forchheimer law for the case of moving porous medium (solid matrix), which means the relative velocity u must be taken instead of the usual $\Phi_l v_l$.

The nonlinear law (38) can be formulated as a Darcy-like law by introducing a velocity–dependent permeability $\hat{K}$ [29]:

$$\hat{K} = \frac{K}{1 + (K^{1/2}\rho_l c_F/\mu)|u|}\,. \tag{39}$$

So (38) is now written in the following form

$$\Phi_l^w(v_l^w - v_s^w) = -\,\frac{\hat{K}}{\mu}\frac{\partial P_l^w}{\partial x}\,.$$

6 One–Phase Model

It is well known that the macroscopic flow behavior at large length scales is well captured by one-phase flow models (see publications on RTM [9, 36, 47]). Such models are sufficiently accurate in predicting flow–front location, mold-filling time and pressure distribution during mold filling.

In this section we consider a one-dimensional model of the injection in a *non-deformable* porous medium (i.e., a rigid preform) with resin as a single phase.

Darcy's Law

Let us assume that the flow is governed by Darcy's law:

$$v = -\frac{K}{\mu}\frac{\partial P_l(x,t)}{\partial x}\,, \tag{40}$$

where $v = \Phi_l v_l$ is the volumetric velocity (i.e., the amount of volume traversing a unit area per unit time through the preform). We also assume that injection is *isothermal*

If the flow is saturated, then the assumption of resin incompressibility (i.e., the mass balance) leads to the following boundary value problem:

$$\begin{cases} \dfrac{\partial v}{\partial x} = 0\,, \\ P_l(0,t) = P_0(t), \quad P_l(x_i(t),t) = P_{atm}\,. \end{cases}$$

We obtain the solution in the explicit form

$$P_l(x,t) = P_0(t) + \frac{P_{atm} - P_0(t)}{x_i(t)}\,x\,. \tag{41}$$

The evolution of the infiltration front is described by the initial value problem

$$\begin{cases} \dfrac{dx_i(t)}{dt} = \dfrac{K}{\mu}\dfrac{P_0(t) - P_{atm}}{x_i(t)}\,, \\ x_i(0) = 0\,, \end{cases}$$

which integrates as

$$x_i^2(t) = \frac{2K}{\mu}\int_0^t (P_0(t) - P_{atm})\,dt\,.$$

If the driving pressure is constant in time (constant pressure driven infiltration) then we obtain the position of the infiltration front as:

$$x_i(t) = \sqrt{\frac{2K}{\mu}\,(P_0 - P_{atm})\;\;t}\,.$$

Determination of the Permeability

The established relationships can be used to evaluate the permeability K, if the positions of the flow front are recorded during the injection experiments and if the fluid viscosity μ is known:

$$K = \frac{\mu\, x_i^2(t)}{2\int_0^t (P_0(t) - P_{atm})\,dt}$$

or

$$K = \frac{\mu\, x_i^2(t)}{2(P_0 - P_{atm})t}\,. \tag{42}$$

We note, that one more relation for the evaluation of the permeability K follows directly from the infiltration front equation

$$K = \frac{\mu\, x_i(t)\, v_l\big(x_i(t),t\big)}{P_0(t) - P_{atm}}\,.$$

On inverse problems for determination of permeabilities. The problem of identification of diffusion coefficient in parabolic or elliptic equations arises in numerous engineering, medical and scientific applications. We want to reconstruct a diffusion coefficient from some additional data on a solution [11, 25, 49]. This data can consist in values of the solution (or functionals of this solution) measured on the boundary or in some points of the time-space region.

Generally, such inverse problems have notorious theoretical and numerical difficulties: non-monotonicity and severe ill–posedness, i.e. the inverse solutions are very sensitive to changes in input data resulting from measurement. Hence, they may not be unique. A regularization method should be used if we want to obtain a stable solution of the inverse problem [13, 17]. We apply such a regularization for determination of the permeability coefficient K in the form of the Least–squares method (see also [7]).

Let the positions of infiltration front $x_i(t_j)$ be recorded at specific time moments t_j, $j = 1, 2, \ldots, J$ during experiment. The objective function is defined as the sum of weighted differences between the front position $\bar{x}_i(t_j)$ predicted from the computational model and its corresponding measured value:

$$S(K) = \sum_{j=1}^{J} c_j \big(x_i(t_j) - \bar{x}_i(t_j)\big)^2 .$$

Identification of the Permeability Coefficient

1. For a given value of K solve the direct problem, describing the liquid moulding process.

2. Compute the objective function $S(K)$ and test the optimality of this value.

3. If the optimal value is not obtained, update the permeability K and goto step 1.

Gradient–type methods or the nonlinear Simplex algorithm can be used to minimize the objective function.

Even if we have an explicit formula (42) for the estimation of the permeability K, the regularization algorithm must be used to overcome the ill-posedness of such estimations due to errors in experimental data. A sta-

ble value of K is obtained taking the mean-value of all estimations:

$$K = \frac{\mu}{2J(P_0 - P_{atm})} \sum_{j=1}^{J} \frac{x_i^2(t_j)}{t_j} \,.$$

Velocity Driven Infiltration

It is well known that the velocity of the infiltration front must not be too slow to ensure a good quality of the final product. If the velocity is too slow it may result in the creation of air bubbles or voids between the fibers.

We can determine the pressure which is sufficient to produce a constant flow rate of the injected resin. Let us consider the following problem

$$\begin{cases} \dfrac{\partial v}{\partial x} = 0 \,, \\ v(0,t) = v_0, \quad P_l(x_i(t),t) = P_{atm} \,. \end{cases}$$

Integration of this equation yields

$$v(x,t) = v_0, \;\; 0 \le x \le x_i(t) \,.$$

Using Darcy's equation and integrating it, we finally get the relation:

$$P_l(0,t) = P_{atm} + \frac{v_0 \mu}{K} \, t \,,$$

i.e. the pressure at the injection line should increase linearly with time.

The Generalized Darcy's Law

In this paragraph we assume that the flow is governed by the generalized Darcy's law (or *power* law):

$$v = \left(-\frac{K^{(1+n)/2}}{\mu \; d_n} \frac{\partial P_l(x,t)}{\partial x} \right)^{1/n} \,. \tag{43}$$

The explicit formula (41) is also valid for this case, thus similarly we obtain that for the generalized Darcy's law the infiltration front is given by

$$x_i(t) = \left(\frac{K^{(1+n)/2}}{\mu \; d_n} (P_0 - P_{atm}) \right)^{1/(n+1)} \left(\frac{n+1}{n} \, t \right)^{n/(n+1)} \,.$$

If front positions $x_i(t)$ are recorded during infiltration experiments, then the permeability K can be evaluated as

$$K = \frac{x_i^2(t)\,(\mu\ d_n)^{2/(n+1)}}{(P_0 - P_{atm})^{2/(n+1)}\,(\frac{n+1}{n}t)^{2n/(n+1)}}\,.$$

The Forchheimer Law

In this paragraph we assume that the flow is governed by the Forchheimer law

$$\frac{\mu}{K}v + \frac{\rho_l\, c_F}{K^{1/2}}\,|v|\,v = -\frac{\partial P_l}{\partial x}\,.$$

First, we will rewrite the formula for the modified permeability $\hat{K}$, when the dependence on velocity is substituted by a pressure gradient dependence (see, also [29]). Taking the absolute values of both sides of the equation and solving for positive root $|v|$, results in

$$|v| = \frac{\mu}{2\rho_l\, c_F K^{1/2}}\left(-1 + \left(1 + 4\gamma K^{3/2}|P'|\right)^{1/2}\right)\,,$$

where we use the notation $P' = \frac{\partial P_l}{\partial x}$ and $\gamma = \frac{\rho_l c_F}{\mu^2}$. Substituting this expression into (39) leads to the relation:

$$v = -\frac{2K}{\mu(1 + (1 + 4\gamma K^{3/2}|P'|)^{1/2}}\frac{\partial P_l(x,t)}{\partial x}\,.$$

The mass balance for the incompressible fluid flow gives the following nonlinear boundary value problem:

$$\begin{cases} \dfrac{\partial}{\partial x}\left(\dfrac{2K}{\mu(1 + (1 + 4\gamma K^{3/2}|P'|)^{1/2}}\dfrac{\partial P_l(x,t)}{\partial x}\right) = 0\,, \\ P_l(0,t) = P_0(t),\ \ P_l(x_i(t),t) = P_{atm}\,. \end{cases} \tag{44}$$

We see that the diffusion is selectively slowed down in places where the gradient of the solution is large. Such nonlinear diffusion problems are used for mathematical modeling of many important processes, e.g. for a nonlinear image processing [28, 33]. The existence and uniqueness of similar initial–boundary value problems is investigated in [6].

In general, solving nonlinear diffusion problem is a very difficult task, but assuming that the flow is saturated (thus K and μ are constant) we again obtain the solution in the following form:

$$P_l(x,t) = P_0(t) + \frac{P_{atm} - P_0(t)}{x_i(t)}\,x\,.$$

The evolution of the infiltration front $x_i(t)$ is described by the initial value problem

$$\begin{cases} \dfrac{dx_i(t)}{dt} = \dfrac{2K/\mu}{1+(1+4\gamma K^{3/2}|\frac{P_0(t)-P_{atm}}{x_i(t)}|)^{1/2}} \dfrac{P_0(t)-P_{atm}}{x_i(t)}\,, \\ x_i(0) = 0\,. \end{cases}$$

Let us consider the constant pressure driven infiltration. Scaling the position of the infiltration front and the time with characteristic constants

$$x_i = 4\gamma K^{3/2}(P_0 - P_{atm})\, X, \quad t = 8\gamma^2 K^2 (P_0 - P_{atm})\mu\, t'$$

the initial value problem for the infiltration front can be rewritten as:

$$\begin{cases} \dfrac{dX^2(t')}{d\,t'} = \dfrac{2}{1+\left(1+\dfrac{1}{X(t')}\right)^{1/2}}\,, \\ X(0) = 0\,. \end{cases}$$

In Figure 1 we plot the computed values of the infiltration front position $X^2(t')$. For the comparison we present also the position of the front obtained by using the Darcy law.

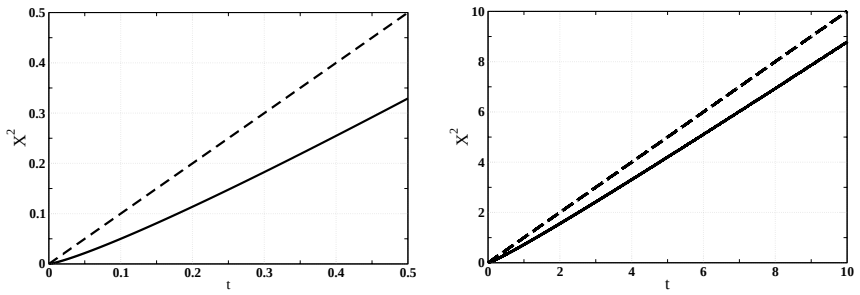

a) b)

Figure 1: Position of $X^2(t)$: a) T = 0.5, b) T= 10. The solid line is a solution of the Forchheimer law, the dashed line is a solution of Darcy's law.

We have investigated the case of the pressure driven infiltration, when the pressure drop is constant. At the beginning the inertial effects are important and the velocity of infiltration front movement is slower for the Forchheimer

law. But as the front moves forward the velocity decreases and the inertial effects become negligible. In this situation the flow again is described by the Darcy law.

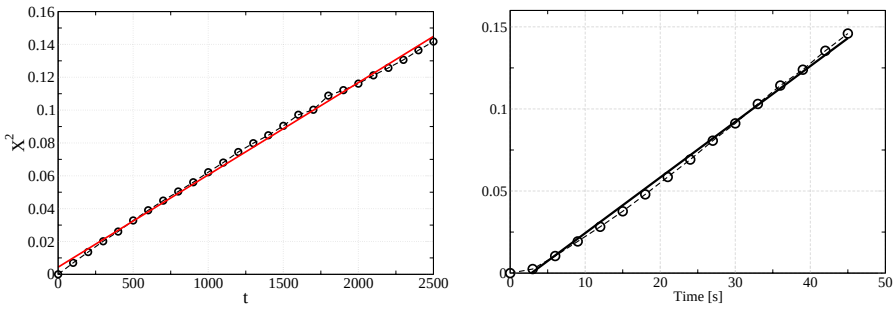

a) b)

Figure 2: Position of $x_i^2(t)$: measured values (circles) and a fitted curve (solid line).

Experimental Data

In this paragraph we present certain results of experimental measurements performed at the Institut fuer Verbundwerkstoffe GmbH, Kaiserslautern. The conditions of the experiment were characterized by a slow flow. A Newtonian liquid was used in experiments. In Figure 2 we plot the measured values of $x_i^2(t)$ (circles) and the linear approximation (solid line), which is fitted to the experimental data using the *Least squares* method. Experiments were done in conditions of pressure driven infiltration and two different values of pressure were used.

The results show that the model based on Darcy's law gives a good approximation of the movement of the infiltration front in this case.

Next we present measurements obtained with non-Newtonian liquids and compare them with our analytical predictions. Three different liquids were used in experiments. In Figure 3 we plot the measured values of $x_i^2(t)$. It can be seen that in two cases the liquids are close to Newtonian liquids and the last one shows a strong non-Newtonian behaviour.

We also estimated the parameter n in the generalized Darcy's law (35).

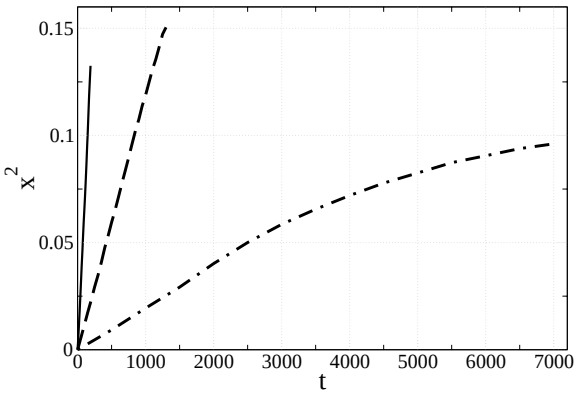

Figure 3: Position of $x_i^2(t)$ for non-Newtonian liquids.

The following technique was used: find n such that

$$M(n) = \min_{n\in[n_s,n_f]} \sum_{k=1}^{M} \big(x_i(t_k) - X_i(t_k,n)\big)^2 ,$$

where $x_i(t_k)$ are measured values of the front position, $X_i(t_k,n)$ are predicted values of the front

$$X_i(t_k,n) = \big(\, a(n)\, t_k + b(n) \,\big)^{\frac{n}{n+1}} ,$$

and $a(n), b(n)$ are obtained by using a linear fitting by the *Least squares* method of the transformed experimental data

$$\big(\, t_k, x_i(t_k)^{\frac{n+1}{n}} \,\big), \quad k = 1, \ldots, M\,.$$

The obtained results are presented in Table 1.

Table 1: The parameter n for non-Newtonian liquids

Liquid	n
$14-1$	1.16
$15-1$	0.975
$15-2$	0.40

It follows from the presented results, that the first and second fluid are very close to Newtonian liquids, but the third liquid can be described only

by the generalized Darcy's law. In Figure 4 we plot the measured values $x_i(t_k)$ (for the third liquid) and predictions of the front position, given by the model based on the generalized Darcy's law with $n = 0.4$.

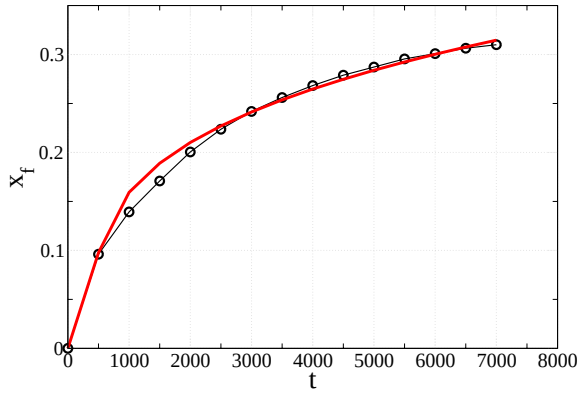

Figure 4: Measured and predicted positions of $x_i(t)$ for a non-Newtonian liquid.

7 Numerical Method

Let us assume that at time $t = 0$ the liquid touches the left border of the preform. We are not trying to describe the early instants of the infiltration process and simply state that the incoming liquid compresses the preform and wets some of its part, therefore the initial positions of the border x_e, as well as of the infiltration front x_i are given *a priori*

$$x_e(0) = x_{e0}, \quad x_i(0) = x_{i0}\,.$$

Then we can identify a wet region D^w and a dry region D^d.

There are two main difficulties in constructing discrete approximations of the given differential problem:

- Moving boundaries $x_e(t)$ and $x_i(t)$ (the Stefan type problem);
- The generalized Darcy's and Forchheinmer laws for flow velocities.

In this section we will analyze some methods for solving the one-dimensional differential problems from above. In order to simplify the presentation we restrict to the mass and momentum balance Eqs. (18)–(21):

$$\begin{cases} \dfrac{\partial \Phi_s^w}{\partial t} + \dfrac{\partial}{\partial x}\left(\Phi_s^w v_s^w\right) = 0\,, \\ \Phi_s^w(x_e(t),t) = \Phi_r, \;\; \Phi_s^w(x_i(t),t) = \Phi_m, \;\; t > 0\,, \\ \Phi_s^w(x,0) = \Phi_0(x), \;\; x_e(t) < x < x_i(t)\,, \\ \dfrac{\partial v_c^w}{\partial x} = 0\,, \\ (1-\Phi_s^w)(v_l^w - v_s^w) = Q\,, \\ \dfrac{\partial P_l^w}{\partial x} = \dfrac{\partial \tau^w}{\partial x}\,. \end{cases} \tag{45}$$

Here, Q describes the Darcy's, generalized Darcy's or Forchheimer's law terms. We assume that the viscosity of the resin is constant during the injection process, i.e. the injection process is finished before the effects of curing reactions and temperature on the viscosity become significant.

7.1 Approximation of the Infiltration Front Equation

The given one-dimensional problem is defined in the region with two free boundaries. Following [1] we define discrete meshes which are dynamically adapted to the moving boundaries:

$$D_h^w = \{\, x_j = x_j(t) : \;\; x_j = x_e(t), + h_w j,\; j = 0, 1, \ldots, M, \;\; x_M = x_i(t) \,\}\,,$$
$$D_h^d = \{\, x_j = x_j(t) : \;\; x_j = x_i(t) + h_d j,\; j = M, M+1, \ldots, N, \;\; x_N = L \,\}\,,$$

here, $M = M(t)$ is selected to preserve the quasi-uniform spatial discretization of the region D

$$M = \frac{\big(x_i(t) - x_e(t)\big)N}{L}, \quad M \geq 1\,.$$

Let τ^n denote the discrete time step at $t = t^n$. In the following, we will denote by Φ_j^n the finite difference approximation of $\Phi_s^w(x_j, t^n)$.

Front Tracking Method

The front tracking method is applied to determine the time step τ_n. Using the free boundary equation for $x_i(t)$, the time step τ_n is chosen such that

the infiltration front jumps from one node to the next node per time step. Thus at time $t = t^n$ the infiltration front position coincides with the node $M^n = n$. The time step τ_n is computed from the discrete approximation of the infiltration front equation.

7.1.1 Pressure Driven Infiltration

Let us consider the pressure driven case. Approximating the differential equation (33) by the forward Euler method yields the equation for the determination of τ_n:

$$\frac{\Phi_s^{d,n+1}(x_i^n + h_w) - \Phi_s^{d,n} x_i^n}{\tau_n} - L\frac{\Phi_s^{d,n+1} - \Phi_s^{d,n}}{\tau_n} = \frac{\Phi^n_{M^n-\frac{1}{2}}}{1 - \Phi^n_{M^n-\frac{1}{2}}} Q(x_{M^n-\frac{1}{2}}, t^n)\,. \tag{46}$$

Then, the inflow velocity u_{in} is computed from (34)

$$u_{in} = \left(L - x_i(t^{n+1})\right)\frac{\Phi_s^{d,n+1} - \Phi_s^{d,n}}{\tau_n} + \left(1 - \Phi_s^{d,n+1}\right)\frac{h_w}{\tau_n}\,.$$

If the pressure drop ΔP_l is constant in time, then these equations can be written in a simpler form:

$$\frac{L - x_e(0)}{N\tau_n} = \frac{\Phi^n_{M^n-\frac{1}{2}}}{(1 - \Phi^n_{M^n-\frac{1}{2}})\Phi_s^d} Q(x_{M^n-\frac{1}{2}}, t^n)\,,$$

$$u_{in} = \left(1 - \Phi_s^{d,n+1}\right)\frac{h_w}{\tau_n}\,.$$

7.1.2 Velocity Driven Infiltration

We will use the fact that the infiltration front moves with the liquid

$$\frac{dx_i(t)}{dt} = u_{in} + \left(\frac{\Phi_s^w}{1 - \Phi_s^w} Q\right)\left(x_i(t), t\right).$$

The time step τ_n is obtained from the discrete equation

$$\frac{h_w}{\tau_n} = u_{in} + \frac{\Phi^n_{M^n-\frac{1}{2}}}{(1 - \Phi^n_{M^n-\frac{1}{2}})} Q(x_{M^n-\frac{1}{2}}, t^n)\,.$$

7.2 Approximation of the Mass Conservation Equations

For a moment, let us assume that the left boundary $x_e(t)$ is not moving, i.e. remains constant. In the case of Darcy's (or Forchheimer's) law we can reduce the system of equations to a single nonlinear parabolic problem [19]

$$\begin{cases} \dfrac{\partial \Phi_s^w}{\partial t} + u_{in}(t)\dfrac{\partial \Phi_s^w}{\partial x} = \dfrac{\partial}{\partial x}\left(\dfrac{K(\Phi_s^w)}{\mu}\,\dfrac{d\Sigma_w(\Phi_s^w)}{d\Phi_s^w}\,\Phi_s^w\,\dfrac{\partial \Phi_s^w}{\partial x}\right), \\ \Phi_s^w(x_e,t) = \Phi_r, \;\; \Phi_s^w(x_i(t),t) = \Phi_m, \;\; t>0\,. \end{cases} \tag{47}$$

Let us introduce the following finite differences notation:

$$\delta_-\Phi_j = \frac{\Phi_j - \Phi_{j-1}}{h}, \quad \delta_+\Phi_j = \frac{\Phi_{j+1}-\Phi_j}{h}\,.$$

The discrete approximation is obtained using the *finite–volume* method. For ease of notation we suppress the superscript index $n+1$ in $M = M^{n+1}$, if it makes no confusion. We use the upwind approximation for the convection part, centered differencing for the diffusion part and a backward Euler method for integration in time. Then, the difference scheme takes the following form

$$\begin{cases} \dfrac{\Phi_j^{n+1} - \tilde{\Phi}_j^n}{\tau_n} + u_{in}^{n+1}\,\delta_-\Phi_j^{n+1} \\ \qquad\qquad = \dfrac{a_{j+0.5}(\Phi^{n+1})\delta_+\Phi_j^{n+1} - a_{j-0.5}(\Phi^{n+1})\delta_-\Phi_j^{n+1}}{h}, \\ a_{j+0.5}(\Phi^{n+1}) = \dfrac{K_{j+0.5}}{\mu}\,\dfrac{d\Sigma_w(\Phi_{j+0.5}^{n+1})}{d\Phi^{n+1}}\,\Phi_{j+0.5}^{n+1}, \\ \Phi_0^{n+1} = \Phi_r, \quad \Phi_M^{n+1} = \Phi_m\,. \end{cases} \tag{48}$$

where

$$\tilde{\Phi}_j^n = \begin{cases} \Phi_j^n, & 1 \le j < M-1\,, \\ \dfrac{1}{2}(\Phi_{M-1}^n + \Phi_M^n), & j = M-1\,. \end{cases}$$

Such a definition of $\tilde{\Phi}_{M-1}^n$ is due to the fact that at $t = t^n$ the elementary finite–volume $V_{M-1} = [x_{M-\frac{3}{2}}, x_{M-\frac{1}{2}}]$ covers the wet and dry region. Therefore, the mass of solid should be computed separately in both regions.

The system of nonlinear equations (48) is solved using Picard linearization, i.e. at each iteration step one gets a system of linear equations:

$$\begin{cases} \dfrac{\Phi_j^{n,r} - \tilde{\Phi}_j^n}{\tau_n} + u_{in}^{n+1}\,\delta_-\Phi_j^{n,r} \\ \qquad\qquad = \dfrac{a_{j+0.5}(\Phi^{n,r-1})\delta_+\Phi_j^{n,r} - a_{j-0.5}(\Phi^{n,r-1})\delta_-\Phi_j^{n,r}}{h}\,, \\ \Phi_0^{n,r} = \Phi_r, \quad \Phi_M^{n,r} = \Phi_m\,, \\ \Phi_j^{n,0} = \Phi_j^n, \quad j = 1, 2, \ldots, M-1\,. \end{cases}$$

Generalized Darcy's Law

The given algorithm can also be used if the flow velocities are described by the generalized Darcy's law, at least when the parameter $n_D < 1$. Here we have changed the notation of n to n_D in formula (43). Then the iterative algorithm has the following form:

$$\frac{\Phi_j^{n,r} - \Phi_j^n}{\tau_n} + u_{in}^{n+1}\,\delta_-\Phi_j^{n,r} = \frac{b_{j+0.5}(\Phi^{n,r-1})\delta_+\Phi_j^{n,r} - b_{j-0.5}(\Phi^{n,r-1})\delta_-\Phi_j^{n,r}}{h}$$

$$b_{j+0.5}(\Phi) = \left(\left(\frac{K^{(1+n_D)/2}(\Phi)}{\mu d_n}\,\frac{d\Sigma_w(\Phi)}{d\Phi} \right)^{\frac{1}{n_D}} \Phi \right)_{j+\frac{1}{2}} |\delta_+\Phi_j|^{(1-n_D)/n_D}\,.$$

7.3 Moving Boundaries

In this section we will take into account that the contact surface $x_e(t)$ is fixed on the solid. Thus if $v_s(x_e(t), t) \neq 0$, the boundary is also moving. Then the position of grid points depends on time and the discrete approximation should be constructed for the case when grid points are moving with its own velocities independent of the velocity of the conservative quantity.

Let us consider the elementary domain, which is described by our mesh $[x_{j-1}(t), x_j(t)]$. We denote by $v = v(x,t)$ the velocity of grid points. Then it is convenient to use the integral formulation of the mass balance equation

$$\frac{\partial \Phi_s^w}{\partial t} + \frac{\partial}{\partial x}\big(v_s^w \Phi_s^w\big) = 0\,.$$

Integrating it over the elementary volume $[x_{j-1}(t), x_j(t)]$ and using the

equality

$$\frac{\partial}{\partial t}\int\limits_{x_{j-1}(t)}^{x_j(t)}\Phi_s^w(x,t)\,dx=\int\limits_{x_{j-1}(t)}^{x_j(t)}\frac{\partial\Phi_s^w}{\partial t}\,dx+\frac{dx_j(t)}{dt}\Phi_s^w(x_j(t),t)$$
$$-\frac{dx_{j-1}(t)}{dt}\Phi_s^w(x_{j-1}(t),t)$$

leads to the integral mass balance equation

$$\frac{\partial}{\partial t}\int\limits_{x_{j-1}(t)}^{x_j(t)}\Phi_s^w(x,t)\,dx+f_j(t)-f_{j-1}(t)=0\,, \tag{49}$$

where

$$f_j(t)=\big(v_s^w(x_j(t),t)-v(x_j(t),t)\big)\Phi_s^w(x_j(t),t)\,.$$

There are many methods for solving equations describing fluid flow problems in a moving coordinate system [4, 24, 30, 42, 46]. They are based on the flux corrected transport idea, when at the first step the equation is solved using some consistent approximation, e.g. the 2-step Lax–Wendroff method [30], then anti-diffusion is added in such a way that the resulting method is still monotonicity preserving. In practical computations the fluxes are limited in a way that no new maxima or minima are generated and the existing extrema are not increased.

Next we present a general algorithm to solve the system of nonlinear partial differential equations (45) on a moving grid. Applying the finite-volume method we approximate the integral equation (49) by the following conservative finite-difference scheme (the nonlinear equations are linearized using the Picard method)

$$\begin{cases}\dfrac{h^{n,r}\Phi_j^{n,r}-h^n\tilde{\Phi}_j^n}{\tau_n}+F\left(w_{j+\frac12}^{n,r},\Phi_{j+1}^{n,r},\Phi_j^{n,r}\right)-F\left(w_{j-\frac12}^{n,r},\Phi_j^{n,r},\Phi_{j-1}^{n,r}\right)\\ \qquad\qquad=a_{j+\frac12}(\Phi^{n,r-1})\delta_+\Phi_j^{n,r}-a_{j-\frac12}(\Phi^{n,r-1})\delta_-\Phi_j^{n,r}\,,\\ w_{j+\frac12}^{n,r}=u_{in}^{n+1}-v_{j+\frac12}^{n,r}\,,\\ \Phi_0^{n,r}=\Phi_r,\quad \Phi_M^{n,r}=\Phi_m\,,\end{cases}$$

where the numerical flux $F\left(w_{j+\frac{1}{2}}, \Phi_{j+1}, \Phi_j\right)$ is defined as follows (see, [14, 27]):

$$F\left(w_{j+\frac{1}{2}}, \Phi_{j+1}, \Phi_j\right) = \frac{1}{2} w_{j+\frac{1}{2}} \left(\Phi_{j+1} + \Phi_j\right) - \frac{1}{2} |w_{j+\frac{1}{2}}| \left(\Phi_{j+1} - \Phi_j\right) .$$

The velocity of the movement of the grid point $x_j(t^n)$ is defined as

$$v_j(t^{n,r}) = v_s^w\big(x_e(t^{n,r}), t^{n,r}\big) \left(1 - \frac{j}{M}\right), \quad j = 0, 1, \ldots, M .$$

7.4 Approximation of the Contact Surface Velocity

We will approximate the equation, which defines the contact surface $x_e(t)$ movement:

$$v_s^w = u_{in} + \frac{K}{\mu} \frac{\partial P_l^w}{\partial x} = u_{in} - \frac{K}{\mu} \frac{d\Sigma_w(\Phi_s^w)}{dx} \frac{\partial \Phi_s^w}{\partial x} .$$

Multiplying it by Φ_s^w we get the full flux:

$$v_s^w \Phi_s^w = u_{in} \Phi_s^w - \frac{K}{\mu} \Phi_s^w \frac{d\Sigma_w(\Phi_s^w)}{dx} \frac{\partial \Phi_s^w}{\partial x} .$$

Taylor's expansion gives the following estimate of the finite difference approximation

$$u_{in} \Phi_{s,1/2}^w - a_{1/2}(\Phi_s^w) \delta_+ \Phi_{s,0}^w = v_{s,0}^w \Phi_{s,0}^w + \frac{h}{2} \Big(u_{in} \frac{\partial \Phi_s^w}{\partial x} - \frac{\partial}{\partial x} \Big(\frac{K}{\mu} \Phi_s^w \frac{d\Sigma_w(\Phi_s^w)}{dx} \frac{\partial \Phi_s^w}{\partial x} \Big) \Big) + O(h^2)$$

or, using the mass conservation equation, one gets

$$u_{in} \Phi_{s,1/2}^w - a_{1/2}(\Phi_s^w) \delta_+ \Phi_{s,0}^w = v_{s,0}^w \Phi_{s,0}^w + \frac{h}{2} \frac{\partial \Phi_{s,0}^w}{\partial t} + O(h^2) .$$

Thus we approximate the contact surface velocity with the high resolution discrete formula

$$v_s^w \left(x_e(t^{n,r})\right) = \frac{u_{in}^{n+1} \Phi_{1/2}^{n,r-1} - a_{1/2}(\Phi^{n,r-1}) \, \delta_+ \Phi_0^{n,r-1}}{\Phi_0^{n,r-1}} + \frac{h^{n,r} - h^n}{2\tau_n} .$$

The contact front position is updated by the following relaxation method:

$$w^{n,r} = \theta w^{n,r-1} + (1-\theta) v_s^w \left(x_e(t^{n,r}), t^{n,r}\right), \quad 0 < \theta < 1 ,$$

$$x_e(t^{n,r}) = x_e(t^n) + \tau_n w^{n,r}, \quad w^{n,0} = 0 .$$

7.5 Analysis of Boundary Conditions

Simulation of liquid polymer moulding requires solving of systems of nonlinear PDEs in domains with moving boundary fronts. Formulation of correct boundary conditions (and development of numerical algorithms for solving such boundary value problems) is still an open problem. In the above analysis we followed papers [18, 19, 21, 39] and prescribed the given values for Φ_s^w on the moving fronts

$$\Phi_s^w\big(x_e(t),t\big) = \Phi_r, \quad \Phi_s^w\big(x_i(t),t\big) = \Phi_m\,.$$

The obtained boundary–value problem is well–defined and a numerical approximation of such boundary conditions is trivial.

But the border x_e is fixed on the solid, therefore it moves with the solid and no boundary condition should be given on it. Let us consider in $Q(t) = [x_e(t), x_i(t)] \times (0,1]$ the following test problem

$$\begin{cases} \dfrac{\partial \Phi}{\partial t} + \dfrac{\partial}{\partial x}\big(v_s(x,t)\Phi\big)\,, \quad (x,t) \in Q(t)\,, \\ \Phi(x,0) = 1, \quad 1 \le x \le 2\,. \end{cases}$$

We assume that both borders are fixed on the solid.

SHASTA algorithm

The method is based on a single flux element in Lagrangian sense with time step τ. The deformed flux element is interpolated to the new grid points at time t^{n+1}.

At $t = 0$ we consider the uniform grid:

$$D_h(t^0) = \Big\{\, x_j^0 :\ x_j^0 = x_e(0) + jh,\ \ j = 0,1,\ldots,M,\ \ h = \frac{1}{M}\,\Big\}\,.$$

At time t^{n+1} the position of each grid point is defined by the movement of the solid:

$$x_j^{n+1} = x_j^n + \tau v_s(x_j^n, t)\,.$$

Let us denote the space step of the obtained nonuniform grid as:

$$h_{j-1/2}^n = x_j^n - x_{j-1}^n\,.$$

The numerical approximation of the solution is computed by the following algorithm (the solution is inversely proportional to the length of the control volume) [4]:

$$\begin{cases} \Phi_0^{n+1} = \dfrac{h_{1/2}^n}{h_{1/2}^{n+1}}\,\Phi_0^n\,, \\ \Phi_j^{n+1} = \dfrac{h_{j-1/2}^n + h_{j+1/2}^n}{h_{j-1/2}^{n+1} + h_{j+1/2}^{n+1}}\,\Phi_j^n, \quad 0 < j < M\,, \\ \Phi_M^{n+1} = \dfrac{h_{M-1/2}^n}{h_{M-1/2}^{n+1}}\,\Phi_M^n\,. \end{cases} \tag{50}$$

We note that the original SHASTA algorithm consists of two stages. During the second stage the corrected values of the solution are obtained by solving the anti–diffusion equation. In the case, when all grid points move with the solid velocity, these two steps can be combined into one. A generalization of the SHASTA algorithm for the case when grid points move with arbitrary velocities is presented in [24].

At the end of this paragraph we will give some remarks on the stability of the SHASTA algorithm. It is explicit and thus the scheme is only conditionally stable. Very small time steps τ may be needed for flows with large velocities. In LPM problems the velocity also depends on the gradient of the solution, thus the Picard–type linearization will lead to an explicit approximation of the parabolic problem.

FVM algorithm

Let us assume that boundary fronts move with the solid, and at each time step we use a uniform grid, i.e. grid points move with velocity $v(x,t)$ different to the solid velocity $v_s(x,t)$.

We use the integral mass conservation equation (49) and apply it to the control volume $[x_e(t), x_{1/2}(t)]$. Since the boundary front $x_e(t)$ moves with the solid part, the mass flux on this boundary is equal to zero and we get the discrete equation

$$\frac{h_{1/2}^{n+1}\Phi_0^{n+1} - h_{1/2}^n\Phi_0^n}{2\tau} + F\big(w_{1/2}, \Phi_1^{n+1}, \Phi_0^{n+1}\big) = 0\,, \tag{51}$$

where $w_{1/2} = v_s^{n+1}(x_{1/2}^{n+1}) - v^{n+1}(x_{1/2}^{n+1})$ and

$$F\left(w_{1/2}, \Phi_1, \Phi_0\right) = \frac{1}{2} w_{1/2}\left(\Phi_1 + \Phi_0\right) - \frac{1}{2}|w_{1/2}|\left(\Phi_1 - \Phi_0\right)\,.$$

Similarly, on the right boundary front we obtain the equation

$$\frac{h_{M-1/2}^{n+1}\Phi_M^{n+1} - h_{M-1/2}^{n}\Phi_M^{n}}{2\tau} - F\big(w_{M-1/2}, \Phi_M^{n+1}, \Phi_{M-1}^{n+1}\big) = 0\,.$$

The obtained approximations of the boundary conditions may lead to linear equations, which do not satisfy the discrete maximum principle. Let us consider the case when $w_{1/2} < 0$, then it follows from (51) that

$$\frac{h_{1/2}^{n+1}\Phi_0^{n+1} - h_{1/2}^{n}\Phi_0^{n}}{2\tau} - |w_{1/2}|\,\Phi_1^{n+1} = 0\,.$$

Computational experiments show that sufficiently small time steps τ should be used, in order to preserve the monotonicity of the solution.

8 Algorithm in Lagrangian Coordinates

One of the main challenges in solving infiltration problems is due to moving fronts, e.g. determination of $x_e(t)$ and $x_i(t)$ and approximation of differential equations and boundary conditions on grids, which are moving in time. An alternative is to formulate the problem in a Lagrangian framework, introducing new coordinates fixed on the solid constituent.

8.1 Reformulation of the Mathematical Model

First, we rewrite all equation of the mathematical model such that the advection terms containing the solid velocity v_s are written explicitly [18] (we will write only equations for a solid matrix and the degree of cure):

$$\frac{\partial \Phi_s^w}{\partial t} + v_s\frac{\partial \Phi_s^w}{\partial x} = \Phi_s^w\frac{\partial}{\partial x}\left(\frac{K}{\mu}\frac{d\Sigma_s(\Phi_s^w)}{d\Phi_s^w}\frac{\partial \Phi_s^w}{\partial x}\right),$$

$$\frac{\partial \delta}{\partial t} + v_s\frac{\partial \delta}{\partial x} = -\frac{1}{1-\Phi_s^w}\frac{K}{\mu}\frac{d\Sigma_s(\Phi_s^w)}{d\Phi_s^w}\frac{\partial \Phi_s^w}{\partial x}\frac{\partial \delta}{\partial x} + f_c(\delta, \theta^w)\,.$$

As reference configuration we consider the configuration in which the solid is dry at rest, i.e. $\Phi_s^w(x) = \Phi_r$. The compression configuration is determined by

$$\frac{\partial x}{\partial \xi} = \frac{\Phi_r}{\Phi_s^w}\,.$$

In Lagrangian coordinates the wet domain reads

$$D^w = \{\xi :\ 0 \le \xi \le \xi_i(t)\}\,,$$

where the left boundary $x_e(t)$ always corresponds to $\xi = 0$. We obtain the following equations for the unknown functions $\Phi_s(\xi,t) = \Phi_s^w(\xi,t)$ and $\delta(\xi,t)$:

$$\frac{\partial \Phi_s}{\partial t} = \frac{\Phi_s^2}{\Phi_r}\frac{\partial}{\partial \xi}\left(Z\,\frac{\partial \Phi_s}{\partial \xi}\right), \tag{52}$$

$$\frac{\partial \delta}{\partial t} = -\frac{\Phi_s}{\Phi_r(1-\Phi_s)} Z\,\frac{\partial \Phi_s}{\partial \xi}\frac{\partial \delta}{\partial \xi} + f_c(\delta,\theta)\,,$$

where

$$Z = \frac{K(\Phi_s)}{\mu}\frac{\Phi_s}{\Phi_r}\frac{d\Sigma_s(\Phi_s)}{d\Phi_s}\,.$$

The infiltration front position is obtained from the equation

$$\frac{\partial \xi_i(t)}{\partial t} = \left(\frac{Z}{1-\Phi_s}\frac{\partial \Phi_s}{\partial \xi}\right)(\xi_i,t)\,, \tag{53}$$

here it is taken into account that the liquid phase velocity with respect to the solid matrix is given by $v_l - v_s$.

8.2 Numerical Algorithm

We introduce the uniform grid

$$D_h^w = \{\xi_j :\ \xi_j = jh,\ j = 0,1,\dots,M(t),\ \xi_M = \xi_i(t)\}\,.$$

The new time step is selected in such a way that the infiltration front moves one space node per time step:

$$\frac{h}{\tau^n} = \frac{Z^n_{M^n-\frac{1}{2}}}{1-\Phi^n_{M^n-\frac{1}{2}}}\,\delta_-\Phi^n_M\,.$$

Here, we assumed that the pressure drop ΔP_l is constant in time.

The mass conservation equation of the solid phase is approximated by the following finite–volume scheme:

$$\begin{cases} \dfrac{\Phi_j^{n,r} - \tilde{\Phi}_j^n}{\tau_n} = \dfrac{(\Phi_j^{n,r-1})^2}{\Phi_r}\,\dfrac{Z_{j+0.5}(\Phi^{n,r-1})\delta_+\Phi_j^{n,r} - Z_{j-0.5}(\Phi^{n,r-1})\delta_-\Phi_j^{n,r}}{h}\,, \\ \Phi_0^{n,r} = \Phi_r, \quad \Phi_M^{n,r} = \Phi_m\,, \\ \Phi_j^{n,0} = \Phi_j^n, \quad j = 1,2,\dots,M-1\,. \end{cases}$$

The position of the free border $x_e(t)$ can be computed integrating the differential equation

$$\frac{dx_e(t)}{dt} = v_s(x_e(t),t)\,.$$

Recall that in a Lagrangian coordinate system this border is fixed at $\xi = 0$.

9 IMPES Type Algorithm

The given nonlinear system of equations can be linearized by solving sequentially the pressure and saturation equations [23]. Applying this iteration method to problem (18)–(21) leads to the following algorithm:

1. *Implicit Pressure Equation*

$$\begin{cases} -\delta_-\delta_+ P^{n,r} = \delta_-\delta_+ \Sigma_w\left(\Phi^{n,r-1}\right), \\ P_0^{n,r} = P_0, \;\; P_M^{n,r} = P_{atm}\,. \end{cases} \tag{54}$$

2. *Mass Balance Equation*

The difference scheme which uses the Enquist-Osher numerical flux [14, 27] has the following conservative form:

$$\begin{cases} \dfrac{\Phi_j^{n,r} - \Phi_j^n}{\tau_n} + \dfrac{F\left(v_{j+\frac{1}{2}}^{n,r}, \Phi_{j+1}^{n,r}, \Phi_j^{n,r}\right) - F\left(v_{j-\frac{1}{2}}^{n,r}, \Phi_j^{n,r}, \Phi_{j-1}^{n,r}\right)}{h} = 0\,, \\ \Phi_0^{n,r} = \Phi_r, \;\; \Phi_M^{n,r} = \Phi_m\,, \end{cases} \tag{55}$$

where the numerical flux F is defined as above.

10 Numerical Experiments

The simulations presented in this section use the values of parameters given in [20], where the infiltration of a thermosetting resin in a network of glass fibers is considered.

The dependence of the permeability on the volume ratio is assumed to be given by

$$K(\Phi_s^w) = K_0 e^{-16(\Phi_s^w - \Phi_r)}\,.$$

The stress-strain relations are given by

$$\Sigma_w(\Phi_s^w) = 0.09\big(e^{26.4\Phi_s^w} - e^{26.4\Phi_r}\big) \quad (\text{Pa})\,,$$
$$\Sigma_d(\Phi_s^d) = 0.3\big(e^{25\Phi_s^d} - e^{25\Phi_r}\big) \quad (\text{Pa})\,,$$

where $\Phi_r = 0.5$ is the undeformed solid phase volume fraction.

The resin viscosity and the function describing the curing process are chosen to be:

$$\mu(\delta,\theta) = \begin{cases} \mu_0 e^{18000/R\theta}\Big(\dfrac{0.1}{0.1-\delta}\Big)^{1.5+\delta} & \text{if } \delta < 0.1\,, \\ \infty & \text{otherwise}\,, \end{cases}$$

$$\mu_0 = 2.78 \cdot 10^{-4}\ (\mathrm{J/mol})\,.$$

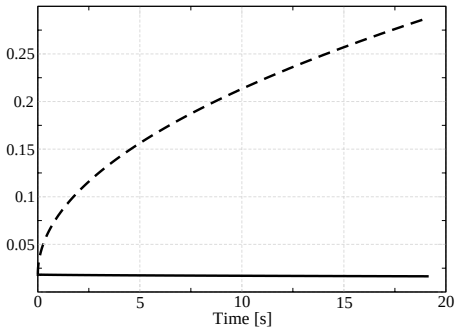

Figure 5: Positions of free boundaries: $x_e(t)$ (solid line) and $x_i(t)$ (dashed line).

In order to test the proposed finite-difference scheme we simulated the infiltration process which is driven by a constant pressure drop of $0.1\,MPa$. After the application of the pressure drop, the preform initially is compressed from $300\,mm$ to $282\,mm$. Figure 5 shows the evolution in time of $x_e(t)$ and $x_i(t)$.

As expected from the one-phase model, the interface $x_i(t)$ moves as $\sqrt{t}$, at least for the initial time interval.

Figure 6 gives the evolution of the solid volume fraction in time.

Acknowledgments

Acknowledgement. This work has been supported from German Science Foundation, DFG, under the grant 269/13-1. One of the authors (RC) has been financially supported by the Lithiuanian State Science and Studies Foundation under the EUREKA project OPTPAPER EU-2623, E-2002.02.07. The authors are grateful to Dr. V.Starikovičius for his valuable suggestions and comments.

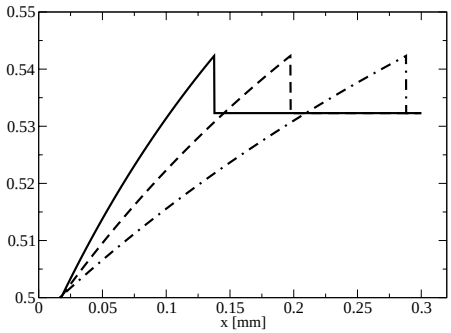

Figure 6: Solid volume fraction $\Phi_s(x,t)$: $t = 3.73$ (solid line), $t = 8.43$ (dashed line), $t = 19.16$ (dotted line).

References

[1] Ambrosi, D., Preziosi, L., Modelling injection moulding processes with deformable porous preforms, *SIAM J. Appl. Math*, **61**, 22-42, 2000.

[2] Beavers, G.S., Spparrow, E.M., Non–Darcy flow through fibrous porous media, *J. Appl. Mech.*, **36**, 711–714 (1969).

[3] Belov, E.B., Lomov, S.V., Verpoest, I., Peters, T., Roose, D., Parnas, R.S., Hoes, K., and Sold, H., Modelling of permeability of textile reinforcements: lattice Boltzmann method, *Composites Science and Techn.*, (2003) (in press).

[4] Boris, J.P., Book, D.L., Flux corrected transport. I. SHASTA, A fluid transport algorithm that works, *J. Comp. Physics*, **11**, 39–69 (1973).

[5] Bruschke, M., Advani, S., Parnas, R., Resin Transfer Moulding in Polymeric Composites, Ch.12 in *Flow and Rheology in Polymer Composites Manufacturing*, Elsevier, pp.465-515, (1994)

[6] Catte, F., Lions, P.L., Morel, J.M., Coll, T., Image selective smoothing and edge detection by nonlinear diffusion, *SIAM J. Numer. Anal.*, **129**, 182–193 (1992).

[7] Chen, H.T., Lin, J.Y., Wu, C.H., Huang, C.H., Numerical algorithm for estimating temperature–dependent thermal conductivity, *Numerical Heat Transfer, B*, **29**(4), 509–522 (1996).

[8] Christopher, R.H., Middleman, S., Power law flow through a packed tube, *Ind. Eng. Chem. Fund.*, **4**, 422–430 (1965).

[9] Chui, W.K., Glimm, J., Tangerman, F.M., Jardine, A.P., Madsen, J.S., Donnellan, T.M., Leek, R., Process modeling in resin transfer molding as a method to enhance product quality, *SIAM Rev.*, **39**, 714–727 (1997).

[10] Čiegis, R., Iliev, O., Numerical algorithms for modeling of liquid polymer moulding, *Mathematical modelling and analysis*, **8**(3), 181–202 (2003).

[11] R. Čiegis, V. Starikovičius, A. Štikonas. Parameters identification algorithms for wood drying modeling. In: A. Buikis, R. Ciegis, A.D. Fitt (eds). *Mathematics in Industry-ECMI Subseries*, Vol.5, *Progress in Industrial Mathematics at ECMI2002*, Springer, Berlin Heidelberg New York, 107–112 (2004).

[12] Clague, D.S., Kandhai, B.D., Zhang, R., Sloot, P.M., Hydraulic permeability of (un)bounded fibrous media using the lattice Boltzmann method, *Physical Review E*, **61**(1), 616–625 (2000).

[13] Engl, H.W., Hanke, M., Neubauer, A., *Regularization of Inverse Problems*, Kluwer, Dondrecht, 1996.

[14] Enquist, B., Osher, S., One-sided difference approximations for nonlinear conservation laws, *Math. Comp.*, **36**, 321–351 (1981).

[15] Ghaddar, C.K., On the permeability of unidirectional fibrous media: a parallel computational approach, *Phys. Fluids*, **7**, 2563–2586 (1995).

[16] Greenkorn, R., *Flow phenomena in porous media. Fundamentals and applications in petroleum, water and food production*, Marcel Dekker, Inc., NY and Basel, 1983.

[17] Hanke, M., Hansen P.C., Regularization methods for large–scale problems, *Surv. Math. Ind.*, **3**, 253–315 (1993).

[18] Farina, A., Preziosi, L., Infiltration process in composite materials manufacturing: modeling and qualitative results, In *Complex flows in industrial processes* (L. Preziosi ed.), Birkhauser, 2000, 281–306.

[19] Farina, A., Preziosi, L., Non-isothermal injection moulding with with resin cure and preform deformability, *Composites A.*, **31**, 1355-1372, (2000)

[20] Farina, A., Preziosi, L., Deformable porous media and composite manufacturing, In *Heterogeneous solids: micromechanics, modelling methods and simulations* (K. Markov, L. Preziosi eds.), Birkhauser, Boston, 2000, 321–410.

[21] Farina, A., Filtration problems in various industrial processes, In *Filtration in porous media and industrial application* (A. Fasano ed.), Springer, 2000, 79–126.

[22] Gebart, B.R., Permeability of unidirectional reinforcements for RTM, *J. of Composite Materials*, **26**(8), 1100-1133, (1992)

[23] Helmig, R., *Multiphase Flow and Transport Processes in the Subsurface*, Springer, Berlin, Heidelberg, 1997.

[24] Hiltunen, K., *Mathematical and Numerical Modelling of Consolidation Processes in Paper Machines*, University of Jyväskylä, Jyväskylä, 1995.

[25] Isakov, V., Kindermann, S., Identification of diffusion coefficient in a one–dimensional parabolic equation, *Inverse Problems*, **16**, 665–680 (2000).

[26] Joseph, D.D., Nield, D.A., Papanicolaou, G., Nonlinear equation governing flow in saturated porous medium, *Water Resources Research*, **18**, 1049–1052 (1982).

[27] Karlsen, K.H., Risebro, N.H., Towers, J.D., Upwind difference approximations for degenerate parabolic convection-diffusion equations with a discontinuous coefficient, *IMA J. Num. Anal.*, **22**, 623–664 (2002).

[28] Kačur, J., Mikula, K., Slow and fast diffusion effects in image processing, *Comput. Visual Sci.*, **3**, 185–195 (2001).

[29] Knupp, P.M., Lage, J.L., Generalization of the Forchheimer–extended Darcy flow model to the tensor permeability case via a variational principle, *J. Fluid Mech.*, **229**, 97–104 (1995).

[30] LeVeque R.J., *Numerical Methods for Conservation Laws*, Birkhäuser Verlag, 1991.

[31] Liu, I.S., On chemical potential and incompressible porous media, *J. Mech.*, **19**, 327–342 (1980).

[32] Mikelic, An., Homogenization theory and applications to filtration through porous media, In *Filtration in porous media and industrial application* (A. Fasano ed.), Springer, 2000, 127–214.

[33] Mikula, K., Ramarosy, N., Semi–implicit finite volume scheme for solving nonlinear diffusion equations in image processing, *Nemer. Math.*, **89**, 561–590 (2001).

[34] Munaf, D., Wineman, S., Rajagopal, K.R., Lee, D.W., A boundary value problem in ground water motion analysis - comparison of the prediction based on Darcy's law and the continuum theory of mixture, *Mat. Models Methods Appl. Sci.*, **3**, 231–248 (1993).

[35] Parnas, R., *Liquid composite moulding*, Hanser Publishers, Munich, 2000.

[36] Parnas, R.S., Phelan, F.R., The effects of heterogenous porous media on mold filing in resin transfer molding, *SAMPLE Quarterly*, **22**, 53–60 (1991).

[37] Pillai, K.M., Advani, S.G., A model for unsaturated flow in woven fiber preforms during mold filling in RTM, *J. of Composite Materials*, **32**(19), 1753–1783 (1998).

[38] Potter, K., *Resin Transfer Moulding*, Chapmann–Hall, 1997.

[39] Preciozi, L., The theory of deformable porous media and its application to composite material manufacturing, *Survey of Mathematics for Industry*, **6**, No.3, 167-214 (1996).

[40] Rasoloarijaona, M., Auriault, J.L., Nonlinear seepage flow through a rigid porous medium, *Eur. J. Mech. B/Fluids*, **13**, 177-195 (1994).

[41] Robitaille, F., Long, A.C., Souter, B.J., Rudd, C.D., Permeability modelling of industrial preforms: simulations and practical aspects, In: *ECCM-9*, Brighton, UK, 2000.

[42] Roe, P.L., Some contributions to the modeling of discontinuous flows. *Lect. Notes Appl. Math.*, **22**, 163-193 (1985)

[43] Rudd, C.D., Long, A.C., Kendall, K.N., and Mangin, C.G., *Liquid Moulding Technologies*, Woodhead Publishing Limited, Cambridge, England, 1997.

[44] Sadiq, T., Advany, S., Parnas, R., Experimental investigation of transverse flow through aligned cylinders, *Int. J. Multiphase Flow*, **21**, No.5, pp.755-774 (1995).

[45] Spelt, P.D., Selerland, T., Lawrence, C.J., and Lee, P.D., Drag coefficient for arrays of cylinders in flows of power–law fluids, *14th Australian Fluid Mechanics Conference, Adelaide, Australia, 10–14 December*, 2001, 881–884.

[46] Sweby, P., High resolution schemes using flux limiters for hyperbolic conservation laws, laws, *SIAM J. Numer. Anal.*, **21**, pp.995-1011 (1984).

[47] Um, M.K., Lee, L.J., A study of the mold filling in resin transfer molding, *Polymer Science and Engineering*, **31**, 765–771 (1991).

[48] Vijaysri, M., Chhabra, R.P., Eswaran, V., Power–law fluid flows across an array of infinite circular cylinders: a numerical study, *J. non–Newt. Fluid Mech.*, **87**, 263–282 (1999).

[49] Weres, J., Olek, W., Guzenda, R., Identification of mathematical model coefficients in the analysis of the heat and mass transport in wood, *Drying Technology*, **18**(8), 1697–1708 (2000).

Published reports of the Fraunhofer ITWM

The PDF-files of the following reports are available under:
www.itwm.fraunhofer.de/rd/presse/berichte

1. D. Hietel, K. Steiner, J. Struckmeier

A Finite - Volume Particle Method for Compressible Flows

We derive a new class of particle methods for conservation laws, which are based on numerical flux functions to model the interactions between moving particles. The derivation is similar to that of classical Finite-Volume methods; except that the fixed grid structure in the Finite-Volume method is substituted by so-called mass packets of particles. We give some numerical results on a shock wave solution for Burgers equation as well as the well-known one-dimensional shock tube problem.
(19 pages, 1998)

2. M. Feldmann, S. Seibold

Damage Diagnosis of Rotors: Application of Hilbert Transform and Multi-Hypothesis Testing

In this paper, a combined approach to damage diagnosis of rotors is proposed. The intention is to employ signal-based as well as model-based procedures for an improved detection of size and location of the damage. In a first step, Hilbert transform signal processing techniques allow for a computation of the signal envelope and the instantaneous frequency, so that various types of non-linearities due to a damage may be identified and classified based on measured response data. In a second step, a multi-hypothesis bank of Kalman Filters is employed for the detection of the size and location of the damage based on the information of the type of damage provided by the results of the Hilbert transform.
Keywords: Hilbert transform, damage diagnosis, Kalman filtering, non-linear dynamics
(23 pages, 1998)

3. Y. Ben-Haim, S. Seibold

Robust Reliability of Diagnostic Multi-Hypothesis Algorithms: Application to Rotating Machinery

Damage diagnosis based on a bank of Kalman filters, each one conditioned on a specific hypothesized system condition, is a well recognized and powerful diagnostic tool. This multi-hypothesis approach can be applied to a wide range of damage conditions. In this paper, we will focus on the diagnosis of cracks in rotating machinery. The question we address is: how to optimize the multi-hypothesis algorithm with respect to the uncertainty of the spatial form and location of cracks and their resulting dynamic effects. First, we formulate a measure of the reliability of the diagnostic algorithm, and then we discuss modifications of the diagnostic algorithm for the maximization of the reliability. The reliability of a diagnostic algorithm is measured by the amount of uncertainty consistent with no-failure of the diagnosis. Uncertainty is quantitatively represented with convex models.
Keywords: Robust reliability, convex models, Kalman filtering, multi-hypothesis diagnosis, rotating machinery, crack diagnosis
(24 pages, 1998)

4. F.-Th. Lentes, N. Siedow

Three-dimensional Radiative Heat Transfer in Glass Cooling Processes

For the numerical simulation of 3D radiative heat transfer in glasses and glass melts, practically applicable mathematical methods are needed to handle such problems optimal using workstation class computers. Since the exact solution would require super-computer capabilities we concentrate on approximate solutions with a high degree of accuracy. The following approaches are studied: 3D diffusion approximations and 3D ray-tracing methods.
(23 pages, 1998)

5. A. Klar, R. Wegener

A hierarchy of models for multilane vehicular traffic
Part I: Modeling

In the present paper multilane models for vehicular traffic are considered. A microscopic multilane model based on reaction thresholds is developed. Based on this model an Enskog like kinetic model is developed. In particular, care is taken to incorporate the correlations between the vehicles. From the kinetic model a fluid dynamic model is derived. The macroscopic coefficients are deduced from the underlying kinetic model. Numerical simulations are presented for all three levels of description in [10]. Moreover, a comparison of the results is given there.
(23 pages, 1998)

Part II: Numerical and stochastic investigations

In this paper the work presented in [6] is continued. The present paper contains detailed numerical investigations of the models developed there. A numerical method to treat the kinetic equations obtained in [6] are presented and results of the simulations are shown. Moreover, the stochastic correlation model used in [6] is described and investigated in more detail.
(17 pages, 1998)

6. A. Klar, N. Siedow

Boundary Layers and Domain Decomposition for Radiative Heat Transfer and Diffusion Equations: Applications to Glass Manufacturing Processes

In this paper domain decomposition methods for radiative transfer problems including conductive heat transfer are treated. The paper focuses on semi-transparent materials, like glass, and the associated conditions at the interface between the materials. Using asymptotic analysis we derive conditions for the coupling of the radiative transfer equations and a diffusion approximation. Several test cases are treated and a problem appearing in glass manufacturing processes is computed. The results clearly show the advantages of a domain decomposition approach. Accuracy equivalent to the solution of the global radiative transfer solution is achieved, whereas computation time is strongly reduced.
(24 pages, 1998)

7. I. Choquet

Heterogeneous catalysis modelling and numerical simulation in rarified gas flows Part I: Coverage locally at equilibrium

A new approach is proposed to model and simulate numerically heterogeneous catalysis in rarefied gas flows. It is developed to satisfy all together the following points:
1) describe the gas phase at the microscopic scale, as required in rarefied flows,
2) describe the wall at the macroscopic scale, to avoid prohibitive computational costs and consider not only crystalline but also amorphous surfaces,
3) reproduce on average macroscopic laws correlated with experimental results and
4) derive analytic models in a systematic and exact way. The problem is stated in the general framework of a non static flow in the vicinity of a catalytic and non porous surface (without aging). It is shown that the exact and systematic resolution method based on the Laplace transform, introduced previously by the author to model collisions in the gas phase, can be extended to the present problem. The proposed approach is applied to the modelling of the EleyRideal and LangmuirHinshelwood recombinations, assuming that the coverage is locally at equilibrium. The models are developed considering one atomic species and extended to the general case of several atomic species. Numerical calculations show that the models derived in this way reproduce with accuracy behaviors observed experimentally.
(24 pages, 1998)

8. J. Ohser, B. Steinbach, C. Lang

Efficient Texture Analysis of Binary Images

A new method of determining some characteristics of binary images is proposed based on a special linear filtering. This technique enables the estimation of the area fraction, the specific line length, and the specific integral of curvature. Furthermore, the specific length of the total projection is obtained, which gives detailed information about the texture of the image. The influence of lateral and directional resolution depending on the size of the applied filter mask is discussed in detail. The technique includes a method of increasing directional resolution for texture analysis while keeping lateral resolution as high as possible.
(17 pages, 1998)

9. J. Orlik

Homogenization for viscoelasticity of the integral type with aging and shrinkage

A multiphase composite with periodic distributed inclusions with a smooth boundary is considered in this contribution. The composite component materials are supposed to be linear viscoelastic and aging (of the nonconvolution integral type, for which the Laplace transform with respect to time is not effectively applicable) and are subjected to isotropic shrinkage. The free shrinkage deformation can be considered as a fictitious temperature deformation in the behavior law. The procedure presented in this paper proposes a way to determine average (effective homogenized) viscoelastic and shrinkage (temperature) composite properties and the homogenized stressfield from known properties of the components. This is done by the extension of the asymptotic homogenization technique known for pure elastic nonhomogeneous bodies to the nonhomogeneous thermoviscoelasticity of the integral noncon-

volution type. Up to now, the homogenization theory has not covered viscoelasticity of the integral type. SanchezPalencia (1980), Francfort & Suquet (1987) (see [2], [9]) have considered homogenization for viscoelasticity of the differential form and only up to the first derivative order. The integralmodeled viscoelasticity is more general then the differential one and includes almost all known differential models. The homogenization procedure is based on the construction of an asymptotic solution with respect to a period of the composite structure. This reduces the original problem to some auxiliary boundary value problems of elasticity and viscoelasticity on the unit periodic cell, of the same type as the original non-homogeneous problem. The existence and uniqueness results for such problems were obtained for kernels satisfying some constrain conditions. This is done by the extension of the Volterra integral operator theory to the Volterra operators with respect to the time, whose 1 kernels are space linear operators for any fixed time variables. Some ideas of such approach were proposed in [11] and [12], where the Volterra operators with kernels depending additionally on parameter were considered. This manuscript delivers results of the same nature for the case of the spaceoperator kernels.
(20 pages, 1998)

10. J. Mohring

Helmholtz Resonators with Large Aperture

The lowest resonant frequency of a cavity resonator is usually approximated by the classical Helmholtz formula. However, if the opening is rather large and the front wall is narrow this formula is no longer valid. Here we present a correction which is of third order in the ratio of the diameters of aperture and cavity. In addition to the high accuracy it allows to estimate the damping due to radiation. The result is found by applying the method of matched asymptotic expansions. The correction contains form factors describing the shapes of opening and cavity. They are computed for a number of standard geometries. Results are compared with numerical computations.
(21 pages, 1998)

11. H. W. Hamacher, A. Schöbel

On Center Cycles in Grid Graphs

Finding "good" cycles in graphs is a problem of great interest in graph theory as well as in locational analysis. We show that the center and median problems are NP hard in general graphs. This result holds both for the variable cardinality case (i.e. all cycles of the graph are considered) and the fixed cardinality case (i.e. only cycles with a given cardinality p are feasible). Hence it is of interest to investigate special cases where the problem is solvable in polynomial time. In grid graphs, the variable cardinality case is, for instance, trivially solvable if the shape of the cycle can be chosen freely. If the shape is fixed to be a rectangle one can analyze rectangles in grid graphs with, in sequence, fixed dimension, fixed cardinality, and variable cardinality. In all cases a complete characterization of the optimal cycles and closed form expressions of the optimal objective values are given, yielding polynomial time algorithms for all cases of center rectangle problems. Finally, it is shown that center cycles can be chosen as rectangles for small cardinalities such that the center cycle problem in grid graphs is in these cases completely solved.
(15 pages, 1998)

12. H. W. Hamacher, K.-H. Küfer

Inverse radiation therapy planning - a multiple objective optimisation approach

For some decades radiation therapy has been proved successful in cancer treatment. It is the major task of clinical radiation treatment planning to realize on the one hand a high level dose of radiation in the cancer tissue in order to obtain maximum tumor control. On the other hand it is obvious that it is absolutely necessary to keep in the tissue outside the tumor, particularly in organs at risk, the unavoidable radiation as low as possible.
No doubt, these two objectives of treatment planning - high level dose in the tumor, low radiation outside the tumor - have a basically contradictory nature. Therefore, it is no surprise that inverse mathematical models with dose distribution bounds tend to be infeasible in most cases. Thus, there is need for approximations compromising between overdosing the organs at risk and underdosing the target volume.
Differing from the currently used time consuming iterative approach, which measures deviation from an ideal (non-achievable) treatment plan using recursively trial-and-error weights for the organs of interest, we go a new way trying to avoid a priori weight choices and consider the treatment planning problem as a multiple objective linear programming problem: with each organ of interest, target tissue as well as organs at risk, we associate an objective function measuring the maximal deviation from the prescribed doses.
We build up a data base of relatively few efficient solutions representing and approximating the variety of Pareto solutions of the multiple objective linear programming problem. This data base can be easily scanned by physicians looking for an adequate treatment plan with the aid of an appropriate online tool.
(14 pages, 1999)

13. C. Lang, J. Ohser, R. Hilfer

On the Analysis of Spatial Binary Images

This paper deals with the characterization of microscopically heterogeneous, but macroscopically homogeneous spatial structures. A new method is presented which is strictly based on integral-geometric formulae such as Crofton's intersection formulae and Hadwiger's recursive definition of the Euler number. The corresponding algorithms have clear advantages over other techniques. As an example of application we consider the analysis of spatial digital images produced by means of Computer Assisted Tomography.
(20 pages, 1999)

14. M. Junk

On the Construction of Discrete Equilibrium Distributions for Kinetic Schemes

A general approach to the construction of discrete equilibrium distributions is presented. Such distribution functions can be used to set up Kinetic Schemes as well as Lattice Boltzmann methods. The general principles are also applied to the construction of Chapman Enskog distributions which are used in Kinetic Schemes for compressible Navier-Stokes equations.
(24 pages, 1999)

15. M. Junk, S. V. Raghurame Rao

A new discrete velocity method for Navier-Stokes equations

The relation between the Lattice Boltzmann Method, which has recently become popular, and the Kinetic Schemes, which are routinely used in Computational Fluid Dynamics, is explored. A new discrete velocity model for the numerical solution of Navier-Stokes equations for incompressible fluid flow is presented by combining both the approaches. The new scheme can be interpreted as a pseudo-compressibility method and, for a particular choice of parameters, this interpretation carries over to the Lattice Boltzmann Method.
(20 pages, 1999)

16. H. Neunzert

Mathematics as a Key to Key Technologies

The main part of this paper will consist of examples, how mathematics really helps to solve industrial problems; these examples are taken from our Institute for Industrial Mathematics, from research in the Technomathematics group at my university, but also from ECMI groups and a company called TecMath, which originated 10 years ago from my university group and has already a very successful history.
(39 pages (4 PDF-Files), 1999)

17. J. Ohser, K. Sandau

Considerations about the Estimation of the Size Distribution in Wicksell's Corpuscle Problem

Wicksell's corpuscle problem deals with the estimation of the size distribution of a population of particles, all having the same shape, using a lower dimensional sampling probe. This problem was originary formulated for particle systems occurring in life sciences but its solution is of actual and increasing interest in materials science. From a mathematical point of view, Wicksell's problem is an inverse problem where the interesting size distribution is the unknown part of a Volterra equation. The problem is often regarded ill-posed, because the structure of the integrand implies unstable numerical solutions. The accuracy of the numerical solutions is considered here using the condition number, which allows to compare different numerical methods with different (equidistant) class sizes and which indicates, as one result, that a finite section thickness of the probe reduces the numerical problems. Furthermore, the relative error of estimation is computed which can be split into two parts. One part consists of the relative discretization error that increases for increasing class size, and the second part is related to the relative statistical error which increases with decreasing class size. For both parts, upper bounds can be given and the sum of them indicates an optimal class width depending on some specific constants.
(18 pages, 1999)

18. E. Carrizosa, H. W. Hamacher, R. Klein, S. Nickel

Solving nonconvex planar location problems by finite dominating sets

It is well-known that some of the classical location problems with polyhedral gauges can be solved in polynomial time by finding a finite dominating set, i. e. a finite set of candidates guaranteed to contain at least one optimal location.
In this paper it is first established that this result holds

for a much larger class of problems than currently considered in the literature. The model for which this result can be proven includes, for instance, location problems with attraction and repulsion, and location-allocation problems.
Next, it is shown that the approximation of general gauges by polyhedral ones in the objective function of our general model can be analyzed with regard to the subsequent error in the optimal objective value. For the approximation problem two different approaches are described, the sandwich procedure and the greedy algorithm. Both of these approaches lead - for fixed epsilon - to polynomial approximation algorithms with accuracy epsilon for solving the general model considered in this paper.
Keywords: Continuous Location, Polyhedral Gauges, Finite Dominating Sets, Approximation, Sandwich Algorithm, Greedy Algorithm
(19 pages, 2000)

19. A. Becker

A Review on Image Distortion Measures

Within this paper we review image distortion measures. A distortion measure is a criterion that assigns a "quality number" to an image. We distinguish between mathematical distortion measures and those distortion measures in-cooperating a priori knowledge about the imaging devices (e. g. satellite images), image processing algorithms or the human physiology. We will consider representative examples of different kinds of distortion measures and are going to discuss them.
Keywords: Distortion measure, human visual system
(26 pages, 2000)

20. H. W. Hamacher, M. Labbé, S. Nickel, T. Sonneborn

Polyhedral Properties of the Uncapacitated Multiple Allocation Hub Location Problem

We examine the feasibility polyhedron of the uncapacitated hub location problem (UHL) with multiple allocation, which has applications in the fields of air passenger and cargo transportation, telecommunication and postal delivery services. In particular we determine the dimension and derive some classes of facets of this polyhedron. We develop some general rules about lifting facets from the uncapacitated facility location (UFL) for UHL and projecting facets from UHL to UFL. By applying these rules we get a new class of facets for UHL which dominates the inequalities in the original formulation. Thus we get a new formulation of UHL whose constraints are all facet–defining. We show its superior computational performance by benchmarking it on a well known data set.
Keywords: integer programming, hub location, facility location, valid inequalities, facets, branch and cut
(21 pages, 2000)

21. H. W. Hamacher, A. Schöbel

Design of Zone Tariff Systems in Public Transportation

Given a public transportation system represented by its stops and direct connections between stops, we consider two problems dealing with the prices for the customers: The fare problem in which subsets of stops are already aggregated to zones and "good" tariffs have to be found in the existing zone system. Closed form solutions for the fare problem are presented for three objective functions. In the zone problem the design of the zones is part of the problem. This problem is NP hard and we therefore propose three heuristics which prove to be very successful in the redesign of one of Germany's transportation systems.
(30 pages, 2001)

22. D. Hietel, M. Junk, R. Keck, D. Teleaga:

The Finite-Volume-Particle Method for Conservation Laws

In the Finite-Volume-Particle Method (FVPM), the weak formulation of a hyperbolic conservation law is discretized by restricting it to a discrete set of test functions. In contrast to the usual Finite-Volume approach, the test functions are not taken as characteristic functions of the control volumes in a spatial grid, but are chosen from a partition of unity with smooth and overlapping partition functions (the particles), which can even move along pre- scribed velocity fields. The information exchange between particles is based on standard numerical flux functions. Geometrical information, similar to the surface area of the cell faces in the Finite-Volume Method and the corresponding normal directions are given as integral quantities of the partition functions. After a brief derivation of the Finite-Volume-Particle Method, this work focuses on the role of the geometric coefficients in the scheme.
(16 pages, 2001)

23. T. Bender, H. Hennes, J. Kalcsics, M. T. Melo, S. Nickel

Location Software and Interface with GIS and Supply Chain Management

The objective of this paper is to bridge the gap between location theory and practice. To meet this objective focus is given to the development of software capable of addressing the different needs of a wide group of users. There is a very active community on location theory encompassing many research fields such as operations research, computer science, mathematics, engineering, geography, economics and marketing. As a result, people working on facility location problems have a very diverse background and also different needs regarding the software to solve these problems. For those interested in non-commercial applications (e. g. students and researchers), the library of location algorithms (LoLA can be of considerable assistance. LoLA contains a collection of efficient algorithms for solving planar, network and discrete facility location problems. In this paper, a detailed description of the functionality of LoLA is presented. In the fields of geography and marketing, for instance, solving facility location problems requires using large amounts of demographic data. Hence, members of these groups (e. g. urban planners and sales managers) often work with geographical information too s. To address the specific needs of these users, LoLA was inked to a geographical information system (GIS) and the details of the combined functionality are described in the paper. Finally, there is a wide group of practitioners who need to solve large problems and require special purpose software with a good data interface. Many of such users can be found, for example, in the area of supply chain management (SCM). Logistics activities involved in strategic SCM include, among others, facility location planning. In this paper, the development of a commercial location software tool is also described. The too is embedded in the Advanced Planner and Optimizer SCM software developed by SAP AG, Walldorf, Germany. The paper ends with some conclusions and an outlook to future activities.
Keywords: facility location, software development, geographical information systems, supply chain management.
(48 pages, 2001)

24. H. W. Hamacher, S. A. Tjandra

Mathematical Modelling of Evacuation Problems: A State of Art

This paper details models and algorithms which can be applied to evacuation problems. While it concentrates on building evacuation many of the results are applicable also to regional evacuation. All models consider the time as main parameter, where the travel time between components of the building is part of the input and the overall evacuation time is the output. The paper distinguishes between macroscopic and microscopic evacuation models both of which are able to capture the evacuees' movement over time.
Macroscopic models are mainly used to produce good lower bounds for the evacuation time and do not consider any individual behavior during the emergency situation. These bounds can be used to analyze existing buildings or help in the design phase of planning a building. Macroscopic approaches which are based on dynamic network flow models (minimum cost dynamic flow, maximum dynamic flow, universal maximum flow, quickest path and quickest flow) are described. A special feature of the presented approach is the fact, that travel times of evacuees are not restricted to be constant, but may be density dependent. Using multicriteria optimization priority regions and blockage due to fire or smoke may be considered. It is shown how the modelling can be done using time parameter either as discrete or continuous parameter.
Microscopic models are able to model the individual evacuee's characteristics and the interaction among evacuees which influence their movement. Due to the corresponding huge amount of data one uses simulation approaches. Some probabilistic laws for individual evacuee's movement are presented. Moreover ideas to model the evacuee's movement using cellular automata (CA) and resulting software are presented. In this paper we will focus on macroscopic models and only summarize some of the results of the microscopic approach. While most of the results are applicable to general evacuation situations, we concentrate on building evacuation.
(44 pages, 2001)

25. J. Kuhnert, S. Tiwari

Grid free method for solving the Poisson equation

A Grid free method for solving the Poisson equation is presented. This is an iterative method. The method is based on the weighted least squares approximation in which the Poisson equation is enforced to be satisfied in every iterations. The boundary conditions can also be enforced in the iteration process. This is a local approximation procedure. The Dirichlet, Neumann and mixed boundary value problems on a unit square are presented and the analytical solutions are compared with the exact solutions. Both solutions matched perfectly.
Keywords: Poisson equation, Least squares method, Grid free method
(19 pages, 2001)

26. T. Götz, H. Rave, D. Reinel-Bitzer, K. Steiner, H. Tiemeier

Simulation of the fiber spinning process

To simulate the influence of process parameters to the melt spinning process a fiber model is used and coupled with CFD calculations of the quench air flow. In the fiber model energy, momentum and mass balance are solved for the polymer mass flow. To calculate the quench air the Lattice Boltzmann method is used. Simulations and experiments for different process parameters and hole configurations are compared and show a good agreement.

Keywords: Melt spinning, fiber model, Lattice Boltzmann, CFD

(19 pages, 2001)

27. A. Zemitis

On interaction of a liquid film with an obstacle

In this paper mathematical models for liquid films generated by impinging jets are discussed. Attention is stressed to the interaction of the liquid film with some obstacle. S. G. Taylor [Proc. R. Soc. London Ser. A 253, 313 (1959)] found that the liquid film generated by impinging jets is very sensitive to properties of the wire which was used as an obstacle. The aim of this presentation is to propose a modification of the Taylor's model, which allows to simulate the film shape in cases, when the angle between jets is different from 180°. Numerical results obtained by discussed models give two different shapes of the liquid film similar as in Taylors experiments. These two shapes depend on the regime: either droplets are produced close to the obstacle or not. The difference between two regimes becomes larger if the angle between jets decreases. Existence of such two regimes can be very essential for some applications of impinging jets, if the generated liquid film can have a contact with obstacles.

Keywords: impinging jets, liquid film, models, numerical solution, shape

(22 pages, 2001)

28. I. Ginzburg, K. Steiner

Free surface lattice-Boltzmann method to model the filling of expanding cavities by Bingham Fluids

The filling process of viscoplastic metal alloys and plastics in expanding cavities is modelled using the lattice Boltzmann method in two and three dimensions. These models combine the regularized Bingham model for viscoplastic with a free-interface algorithm. The latter is based on a modified immiscible lattice Boltzmann model in which one species is the fluid and the other one is considered as vacuum. The boundary conditions at the curved liquid-vacuum interface are met without any geometrical front reconstruction from a first-order Chapman-Enskog expansion. The numerical results obtained with these models are found in good agreement with available theoretical and numerical analysis.

Keywords: Generalized LBE, free-surface phenomena, interface boundary conditions, filling processes, Bingham viscoplastic model, regularized models

(22 pages, 2001)

29. H. Neunzert

»Denn nichts ist für den Menschen als Menschen etwas wert, was er nicht mit Leidenschaft tun kann«

Vortrag anlässlich der Verleihung des Akademiepreises des Landes Rheinland-Pfalz am 21.11.2001

Was macht einen guten Hochschullehrer aus? Auf diese Frage gibt es sicher viele verschiedene, fachbezogene Antworten, aber auch ein paar allgemeine Gesichtspunkte: es bedarf der »Leidenschaft« für die Forschung (Max Weber), aus der dann auch die Begeisterung für die Lehre erwächst. Forschung und Lehre gehören zusammen, um die Wissenschaft als lebendiges Tun vermitteln zu können. Der Vortrag gibt Beispiele dafür, wie in angewandter Mathematik Forschungsaufgaben aus praktischen Alltagsproblemstellungen erwachsen, die in die Lehre auf verschiedenen Stufen (Gymnasium bis Graduiertenkolleg) einfließen; er leitet damit auch zu einem aktuellen Forschungsgebiet, der Mehrskalenanalyse mit ihren vielfältigen Anwendungen in Bildverarbeitung, Materialentwicklung und Strömungsmechanik über, was aber nur kurz gestreift wird. Mathematik erscheint hier als eine moderne Schlüsseltechnologie, die aber auch enge Beziehungen zu den Geistes- und Sozialwissenschaften hat.

Keywords: Lehre, Forschung, angewandte Mathematik, Mehrskalenanalyse, Strömungsmechanik

(18 pages, 2001)

30. J. Kuhnert, S. Tiwari

Finite pointset method based on the projection method for simulations of the incompressible Navier-Stokes equations

A Lagrangian particle scheme is applied to the projection method for the incompressible Navier-Stokes equations. The approximation of spatial derivatives is obtained by the weighted least squares method. The pressure Poisson equation is solved by a local iterative procedure with the help of the least squares method. Numerical tests are performed for two dimensional cases. The Couette flow, Poiseuelle flow, decaying shear flow and the driven cavity flow are presented. The numerical solutions are obtained for stationary as well as instationary cases and are compared with the analytical solutions for channel flows. Finally, the driven cavity in a unit square is considered and the stationary solution obtained from this scheme is compared with that from the finite element method.

Keywords: Incompressible Navier-Stokes equations, Meshfree method, Projection method, Particle scheme, Least squares approximation

AMS subject classification: 76D05, 76M28

(25 pages, 2001)

31. R. Korn, M. Krekel

Optimal Portfolios with Fixed Consumption or Income Streams

We consider some portfolio optimisation problems where either the investor has a desire for an a priori specified consumption stream or/and follows a deterministic pay in scheme while also trying to maximize expected utility from final wealth. We derive explicit closed form solutions for continuous and discrete monetary streams. The mathematical method used is classical stochastic control theory.

Keywords: Portfolio optimisation, stochastic control, HJB equation, discretisation of control problems.

(23 pages, 2002)

32. M. Krekel

Optimal portfolios with a loan dependent credit spread

If an investor borrows money he generally has to pay higher interest rates than he would have received, if he had put his funds on a savings account. The classical model of continuous time portfolio optimisation ignores this effect. Since there is obviously a connection between the default probability and the total percentage of wealth, which the investor is in debt, we study portfolio optimisation with a control dependent interest rate. Assuming a logarithmic and a power utility function, respectively, we prove explicit formulae of the optimal control.

Keywords: Portfolio optimisation, stochastic control, HJB equation, credit spread, log utility, power utility, non-linear wealth dynamics

(25 pages, 2002)

33. J. Ohser, W. Nagel, K. Schladitz

The Euler number of discretized sets - on the choice of adjacency in homogeneous lattices

Two approaches for determining the Euler-Poincaré characteristic of a set observed on lattice points are considered in the context of image analysis { the integral geometric and the polyhedral approach. Information about the set is assumed to be available on lattice points only. In order to retain properties of the Euler number and to provide a good approximation of the true Euler number of the original set in the Euclidean space, the appropriate choice of adjacency in the lattice for the set and its background is crucial. Adjacencies are defined using tessellations of the whole space into polyhedrons. In R 3 , two new 14 adjacencies are introduced additionally to the well known 6 and 26 adjacencies. For the Euler number of a set and its complement, a consistency relation holds. Each of the pairs of adjacencies (14:1; 14:1), (14:2; 14:2), (6; 26), and (26; 6) is shown to be a pair of complementary adjacencies with respect to this relation. That is, the approximations of the Euler numbers are consistent if the set and its background (complement) are equipped with this pair of adjacencies. Furthermore, sufficient conditions for the correctness of the approximations of the Euler number are given. The analysis of selected microstructures and a simulation study illustrate how the estimated Euler number depends on the chosen adjacency. It also shows that there is not a uniquely best pair of adjacencies with respect to the estimation of the Euler number of a set in Euclidean space.

Keywords: image analysis, Euler number, neighborhod relationships, cuboidal lattice

(32 pages, 2002)

34. I. Ginzburg, K. Steiner

Lattice Boltzmann Model for Free-Surface flow and Its Application to Filling Process in Casting

A generalized lattice Boltzmann model to simulate free-surface is constructed in both two and three dimensions. The proposed model satisfies the interfacial boundary conditions accurately. A distinctive feature of the model is that the collision processes is carried out only on the points occupied partially or fully by the fluid. To maintain a sharp interfacial front, the method includes an anti-diffusion algorithm. The unknown distribution functions at the interfacial region are constructed according to the first order Chapman-Enskog analysis. The interfacial boundary conditions are satis-

fied exactly by the coefficients in the Chapman-Enskog expansion. The distribution functions are naturally expressed in the local interfacial coordinates. The macroscopic quantities at the interface are extracted from the least-square solutions of a locally linearized system obtained from the known distribution functions. The proposed method does not require any geometric front construction and is robust for any interfacial topology. Simulation results of realistic filling process are presented: rectangular cavity in two dimensions and Hammer box, Campbell box, Sheffield box, and Motorblock in three dimensions. To enhance the stability at high Reynolds numbers, various upwind-type schemes are developed. Free-slip and no-slip boundary conditions are also discussed.
Keywords: Lattice Boltzmann models; free-surface phenomena; interface boundary conditions; filling processes; injection molding; volume of fluid method; interface boundary conditions; advection-schemes; upwind-schemes
(54 pages, 2002)

35. M. Günther, A. Klar, T. Materne, R. Wegener

Multivalued fundamental diagrams and stop and go waves for continuum traffic equations

In the present paper a kinetic model for vehicular traffic leading to multivalued fundamental diagrams is developed and investigated in detail. For this model phase transitions can appear depending on the local density and velocity of the flow. A derivation of associated macroscopic traffic equations from the kinetic equation is given. Moreover, numerical experiments show the appearance of stop and go waves for highway traffic with a bottleneck.
Keywords: traffic flow, macroscopic equations, kinetic derivation, multivalued fundamental diagram, stop and go waves, phase transitions
(25 pages, 2002)

36. S. Feldmann, P. Lang, D. Prätzel-Wolters

Parameter influence on the zeros of network determinants

To a network N(q) with determinant D(s;q) depending on a parameter vector $q \hat{I} R^r$ via identification of some of its vertices, a network N^ (q) is assigned. The paper deals with procedures to find N^ (q), such that its determinant D^ (s;q) admits a factorization in the determinants of appropriate subnetworks, and with the estimation of the deviation of the zeros of D^ from the zeros of D. To solve the estimation problem state space methods are applied.
Keywords: Networks, Equicofactor matrix polynomials, Realization theory, Matrix perturbation theory
(30 pages, 2002)

37. K. Koch, J. Ohser, K. Schladitz

Spectral theory for random closed sets and estimating the covariance via frequency space

A spectral theory for stationary random closed sets is developed and provided with a sound mathematical basis. Definition and proof of existence of the Bartlett spectrum of a stationary random closed set as well as the proof of a Wiener-Khintchine theorem for the power spectrum are used to two ends: First, well known second order characteristics like the covariance can be estimated faster than usual via frequency space. Second, the Bartlett spectrum and the power spectrum can be used as second order characteristics in frequency space. Examples show, that in some cases information about the random closed set is easier to obtain from these characteristics in frequency space than from their real world counterparts.
Keywords: Random set, Bartlett spectrum, fast Fourier transform, power spectrum
(28 pages, 2002)

38. D. d'Humières, I. Ginzburg

Multi-reflection boundary conditions for lattice Boltzmann models

We present a unified approach of several boundary conditions for lattice Boltzmann models. Its general framework is a generalization of previously introduced schemes such as the bounce-back rule, linear or quadratic interpolations, etc. The objectives are two fold: first to give theoretical tools to study the existing boundary conditions and their corresponding accuracy; secondly to design formally third- order accurate boundary conditions for general flows. Using these boundary conditions, Couette and Poiseuille flows are exact solution of the lattice Boltzmann models for a Reynolds number $Re = 0$ (Stokes limit).
Numerical comparisons are given for Stokes flows in periodic arrays of spheres and cylinders, linear periodic array of cylinders between moving plates and for Navier-Stokes flows in periodic arrays of cylinders for $Re < 200$. These results show a significant improvement of the overall accuracy when using the linear interpolations instead of the bounce-back reflection (up to an order of magnitude on the hydrodynamics fields). Further improvement is achieved with the new multi-reflection boundary conditions, reaching a level of accuracy close to the quasi-analytical reference solutions, even for rather modest grid resolutions and few points in the narrowest channels. More important, the pressure and velocity fields in the vicinity of the obstacles are much smoother with multi-reflection than with the other boundary conditions.
Finally the good stability of these schemes is highlighted by some simulations of moving obstacles: a cylinder between flat walls and a sphere in a cylinder.
Keywords: lattice Boltzmann equation, boudary condistions, bounce-back rule, Navier-Stokes equation
(72 pages, 2002)

39. R. Korn

Elementare Finanzmathematik

Im Rahmen dieser Arbeit soll eine elementar gehaltene Einführung in die Aufgabenstellungen und Prinzipien der modernen Finanzmathematik gegeben werden. Insbesondere werden die Grundlagen der Modellierung von Aktienkursen, der Bewertung von Optionen und der Portfolio-Optimierung vorgestellt. Natürlich können die verwendeten Methoden und die entwickelte Theorie nicht in voller Allgemeinheit für den Schulunterricht verwendet werden, doch sollen einzelne Prinzipien so heraus gearbeitet werden, dass sie auch an einfachen Beispielen verstanden werden können.
Keywords: Finanzmathematik, Aktien, Optionen, Portfolio-Optimierung, Börse, Lehrerweiterbildung, Mathematikunterricht
(98 pages, 2002)

40. J. Kallrath, M. C. Müller, S. Nickel

Batch Presorting Problems: Models and Complexity Results

In this paper we consider short term storage systems. We analyze presorting strategies to improve the effiency of these storage systems. The presorting task is called Batch PreSorting Problem (BPSP). The BPSP is a variation of an assigment problem, i. e., it has an assigment problem kernel and some additional constraints. We present different types of these presorting problems, introduce mathematical programming formulations and prove the NP-completeness for one type of the BPSP. Experiments are carried out in order to compare the different model formulations and to investigate the behavior of these models.
Keywords: Complexity theory, Integer programming, Assigment, Logistics
(19 pages, 2002)

41. J. Linn

On the frame-invariant description of the phase space of the Folgar-Tucker equation

The Folgar-Tucker equation is used in flow simulations of fiber suspensions to predict fiber orientation depending on the local flow. In this paper, a complete, frame-invariant description of the phase space of this differential equation is presented for the first time.
Key words: fiber orientation, Folgar-Tucker equation, injection molding
(5 pages, 2003)

42. T. Hanne, S. Nickel

A Multi-Objective Evolutionary Algorithm for Scheduling and Inspection Planning in Software Development Projects

In this article, we consider the problem of planning inspections and other tasks within a software development (SD) project with respect to the objectives quality (no. of defects), project duration, and costs. Based on a discrete-event simulation model of SD processes comprising the phases coding, inspection, test, and rework, we present a simplified formulation of the problem as a multiobjective optimization problem. For solving the problem (i. e. finding an approximation of the efficient set) we develop a multiobjective evolutionary algorithm. Details of the algorithm are discussed as well as results of its application to sample problems.
Key words: multiple objective programming, project management and scheduling, software development, evolutionary algorithms, efficient set
(29 pages, 2003)

43. T. Bortfeld , K.-H. Küfer, M. Monz, A. Scherrer, C. Thieke, H. Trinkaus

Intensity-Modulated Radiotherapy - A Large Scale Multi-Criteria Programming Problem -

Radiation therapy planning is always a tight rope walk between dangerous insufficient dose in the target volume and life threatening overdosing of organs at risk. Finding ideal balances between these inherently contradictory goals challenges dosimetrists and physicians in their daily practice. Today's planning systems are typically based on a single evaluation function that measures the quality of a radiation treatment plan. Unfortunately, such a one dimensional approach can-

not satisfactorily map the different backgrounds of physicians and the patient dependent necessities. So, too often a time consuming iteration process between evaluation of dose distribution and redefinition of the evaluation function is needed.
In this paper we propose a generic multi-criteria approach based on Pareto's solution concept. For each entity of interest - target volume or organ at risk a structure dependent evaluation function is defined measuring deviations from ideal doses that are calculated from statistical functions. A reasonable bunch of clinically meaningful Pareto optimal solutions are stored in a data base, which can be interactively searched by physicians. The system guarantees dynamical planning as well as the discussion of tradeoffs between different entities.
Mathematically, we model the upcoming inverse problem as a multi-criteria linear programming problem. Because of the large scale nature of the problem it is not possible to solve the problem in a 3D-setting without adaptive reduction by appropriate approximation schemes.
Our approach is twofold: First, the discretization of the continuous problem is based on an adaptive hierarchical clustering process which is used for a local refinement of constraints during the optimization procedure. Second, the set of Pareto optimal solutions is approximated by an adaptive grid of representatives that are found by a hybrid process of calculating extreme compromises and interpolation methods.
Keywords: multiple criteria optimization, representative systems of Pareto solutions, adaptive triangulation, clustering and disaggregation techniques, visualization of Pareto solutions, medical physics, external beam radiotherapy planning, intensity modulated radiotherapy
(31 pages, 2003)

44. T. Halfmann, T. Wichmann

Overview of Symbolic Methods in Industrial Analog Circuit Design

Industrial analog circuits are usually designed using numerical simulation tools. To obtain a deeper circuit understanding, symbolic analysis techniques can additionally be applied. Approximation methods which reduce the complexity of symbolic expressions are needed in order to handle industrial-sized problems. This paper will give an overview to the field of symbolic analog circuit analysis. Starting with a motivation, the state-of-the-art simplification algorithms for linear as well as for nonlinear circuits are presented. The basic ideas behind the different techniques are described, whereas the technical details can be found in the cited references. Finally, the application of linear and nonlinear symbolic analysis will be shown on two example circuits.
Keywords: CAD, automated analog circuit design, symbolic analysis, computer algebra, behavioral modeling, system simulation, circuit sizing, macro modeling, differential-algebraic equations, index
(17 pages, 2003)

45. S. E. Mikhailov, J. Orlik

Asymptotic Homogenisation in Strength and Fatigue Durability Analysis of Composites

Asymptotic homogenisation technique and two-scale convergence is used for analysis of macro-strength and fatigue durability of composites with a periodic structure under cyclic loading. The linear damage accumulation rule is employed in the phenomenological micro-durability conditions (for each component of the composite) under varying cyclic loading. Both local and non-local strength and durability conditions are analysed. The strong convergence of the strength and fatigue damage measure as the structure period tends to zero is proved and their limiting values are estimated.
Keywords: multiscale structures, asymptotic homogenization, strength, fatigue, singularity, non-local conditions
(14 pages, 2003)

46. P. Domínguez-Marín, P. Hansen, N. Mladenović, S. Nickel

Heuristic Procedures for Solving the Discrete Ordered Median Problem

We present two heuristic methods for solving the Discrete Ordered Median Problem (DOMP), for which no such approaches have been developed so far. The DOMP generalizes classical discrete facility location problems, such as the p-median, p-center and Uncapacitated Facility Location problems. The first procedure proposed in this paper is based on a genetic algorithm developed by Moreno Vega [MV96] for p-median and p-center problems. Additionally, a second heuristic approach based on the Variable Neighborhood Search metaheuristic (VNS) proposed by Hansen & Mladenovic [HM97] for the p-median problem is described. An extensive numerical study is presented to show the efficiency of both heuristics and compare them.
Keywords: genetic algorithms, variable neighborhood search, discrete facility location
(31 pages, 2003)

47. N. Boland, P. Domínguez-Marín, S. Nickel, J. Puerto

Exact Procedures for Solving the Discrete Ordered Median Problem

The Discrete Ordered Median Problem (DOMP) generalizes classical discrete location problems, such as the N-median, N-center and Uncapacitated Facility Location problems. It was introduced by Nickel [16], who formulated it as both a nonlinear and a linear integer program. We propose an alternative integer linear programming formulation for the DOMP, discuss relationships between both integer linear programming formulations, and show how properties of optimal solutions can be used to strengthen these formulations. Moreover, we present a specific branch and bound procedure to solve the DOMP more efficiently. We test the integer linear programming formulations and this branch and bound method computationally on randomly generated test problems.
Keywords: discrete location, Integer programming
(41 pages, 2003)

48. S. Feldmann, P. Lang

Padé-like reduction of stable discrete linear systems preserving their stability

A new stability preserving model reduction algorithm for discrete linear SISO-systems based on their impulse response is proposed. Similar to the Padé approximation, an equation system for the Markov parameters involving the Hankel matrix is considered, that here however is chosen to be of very high dimension. Although this equation system therefore in general cannot be solved exactly, it is proved that the approximate solution, computed via the Moore-Penrose inverse, gives rise to a stability preserving reduction scheme, a property that cannot be guaranteed for the Padé approach. Furthermore, the proposed algorithm is compared to another stability preserving reduction approach, namely the balanced truncation method, showing comparable performance of the reduced systems. The balanced truncation method however starts from a state space description of the systems and in general is expected to be more computational demanding.
Keywords: Discrete linear systems, model reduction, stability, Hankel matrix, Stein equation
(16 pages, 2003)

49. J. Kallrath, S. Nickel

A Polynomial Case of the Batch Presorting Problem

This paper presents new theoretical results for a special case of the batch presorting problem (BPSP). We will show tht this case can be solved in polynomial time. Offline and online algorithms are presented for solving the BPSP. Competetive analysis is used for comparing the algorithms.
Keywords: batch presorting problem, online optimization, competetive analysis, polynomial algorithms, logistics
(17 pages, 2003)

50. T. Hanne, H. L. Trinkaus

knowCube for MCDM – Visual and Interactive Support for Multicriteria Decision Making

In this paper, we present a novel multicriteria decision support system (MCDSS), called knowCube, consisting of components for knowledge organization, generation, and navigation. Knowledge organization rests upon a database for managing qualitative and quantitative criteria, together with add-on information. Knowledge generation serves filling the database via e. g. identification, optimization, classification or simulation. For "finding needles in haycocks", the knowledge navigation component supports graphical database retrieval and interactive, goal-oriented problem solving. Navigation "helpers" are, for instance, cascading criteria aggregations, modifiable metrics, ergonomic interfaces, and customizable visualizations. Examples from real-life projects, e.g. in industrial engineering and in the life sciences, illustrate the application of our MCDSS.
Key words: Multicriteria decision making, knowledge management, decision support systems, visual interfaces, interactive navigation, real-life applications.
(26 pages, 2003)

51. O. Iliev, V. Laptev

On Numerical Simulation of Flow Through Oil Filters

This paper concerns numerical simulation of flow through oil filters. Oil filters consist of filter housing (filter box), and a porous filtering medium, which completely separates the inlet from the outlet. We discuss mathematical models, describing coupled flows in the pure liquid subregions and in the porous filter media, as well as interface conditions between them. Further, we reformulate the problem in fictitious regions method manner, and discuss peculiarities of the numerical algorithm in solving the coupled system. Next, we show numerical results, validating the model and the

algorithm. Finally, we present results from simulation of 3-D oil flow through a real car filter.
Keywords: oil filters, coupled flow in plain and porous media, Navier-Stokes, Brinkman, numerical simulation
(8 pages, 2003)

52. W. Dörfler, O. Iliev, D. Stoyanov, D. Vassileva

On a Multigrid Adaptive Refinement Solver for Saturated Non-Newtonian Flow in Porous Media

A multigrid adaptive refinement algorithm for non-Newtonian flow in porous media is presented. The saturated flow of a non-Newtonian fluid is described by the continuity equation and the generalized Darcy law. The resulting second order nonlinear elliptic equation is discretized by a finite volume method on a cell-centered grid. A nonlinear full-multigrid, full-approximation-storage algorithm is implemented. As a smoother, a single grid solver based on Picard linearization and Gauss-Seidel relaxation is used. Further, a local refinement multigrid algorithm on a composite grid is developed. A residual based error indicator is used in the adaptive refinement criterion. A special implementation approach is used, which allows us to perform unstructured local refinement in conjunction with the finite volume discretization. Several results from numerical experiments are presented in order to examine the performance of the solver.
Keywords: Nonlinear multigrid, adaptive refinement, non-Newtonian flow in porous media
(17 pages, 2003)

53. S. Kruse

On the Pricing of Forward Starting Options under Stochastic Volatility

We consider the problem of pricing European forward starting options in the presence of stochastic volatility. By performing a change of measure using the asset price at the time of strike determination as a numeraire, we derive a closed-form solution based on Heston's model of stochastic volatility.
Keywords: Option pricing, forward starting options, Heston model, stochastic volatility, cliquet options
(11 pages, 2003)

54. O. Iliev, D. Stoyanov

Multigrid – adaptive local refinement solver for incompressible flows

A non-linear multigrid solver for incompressible Navier-Stokes equations, exploiting finite volume discretization of the equations, is extended by adaptive local refinement. The multigrid is the outer iterative cycle, while the SIMPLE algorithm is used as a smoothing procedure. Error indicators are used to define the refinement subdomain. A special implementation approach is used, which allows to perform unstructured local refinement in conjunction with the finite volume discretization. The multigrid - adaptive local refinement algorithm is tested on 2D Poisson equation and further is applied to a lid-driven flows in a cavity (2D and 3D case), comparing the results with bench-mark data. The software design principles of the solver are also discussed.
Keywords: Navier-Stokes equations, incompressible flow, projection-type splitting, SIMPLE, multigrid methods, adaptive local refinement, lid-driven flow in a cavity
(37 pages, 2003)

55. V. Starikovicius

The multiphase flow and heat transfer in porous media

In first part of this work, summaries of traditional Multiphase Flow Model and more recent Multiphase Mixture Model are presented. Attention is being paid to attempts include various heterogeneous aspects into models. In second part, MMM based differential model for two-phase immiscible flow in porous media is considered. A numerical scheme based on the sequential solution procedure and control volume based finite difference schemes for the pressure and saturation-conservation equations is developed. A computer simulator is built, which exploits object-oriented programming techniques. Numerical result for several test problems are reported.
Keywords: Two-phase flow in porous media, various formulations, global pressure, multiphase mixture model, numerical simulation
(30 pages, 2003)

56. P. Lang, A. Sarishvili, A. Wirsen

Blocked neural networks for knowledge extraction in the software development process

One of the main goals of an organization developing software is to increase the quality of the software while at the same time to decrease the costs and the duration of the development process. To achieve this, various decisions e.ecting this goal before and during the development process have to be made by the managers. One appropriate tool for decision support are simulation models of the software life cycle, which also help to understand the dynamics of the software development process. Building up a simulation model requires a mathematical description of the interactions between di.erent objects involved in the development process. Based on experimental data, techniques from the .eld of knowledge discovery can be used to quantify these interactions and to generate new process knowledge based on the analysis of the determined relationships. In this paper blocked neuronal networks and related relevance measures will be presented as an appropriate tool for quanti.cation and validation of qualitatively known dependencies in the software development process.
Keywords: Blocked Neural Networks, Nonlinear Regression, Knowledge Extraction, Code Inspection
(21 pages, 2003)

57. H. Knaf, P. Lang, S. Zeiser

Diagnosis aiding in Regulation Thermography using Fuzzy Logic

The objective of the present article is to give an overview of an application of Fuzzy Logic in Regulation Thermography, a method of medical diagnosis support. An introduction to this method of the complementary medical science based on temperature measurements – so-called thermograms – is provided. The process of modelling the physician's thermogram evaluation rules using the calculus of Fuzzy Logic is explained.
Keywords: fuzzy logic,knowledge representation, expert system
(22 pages, 2003)

58. M.T. Melo, S. Nickel, F. Saldanha da Gama

Largescale models for dynamic multi-commodity capacitated facility location

In this paper we focus on the strategic design of supply chain networks. We propose a mathematical modeling framework that captures many practical aspects of network design problems simultaneously but which have not received adequate attention in the literature. The aspects considered include: dynamic planning horizon, generic supply chain network structure, external supply of materials, inventory opportunities for goods, distribution of commodities, facility configuration, availability of capital for investments, and storage limitations. Moreover, network configuration decisions concerning the gradual relocation of facilities over the planning horizon are considered. To cope with fluctuating demands, capacity expansion and reduction scenarios are also analyzed as well as modular capacity shifts. The relation of the proposed modeling framework with existing models is discussed. For problems of reasonable size we report on our computational experience with standard mathematical programming software. In particular, useful insights on the impact of various factors on network design decisions are provided.
Keywords: supply chain management, strategic planning, dynamic location, modeling
(40 pages, 2003)

59. J. Orlik

Homogenization for contact problems with periodically rough surfaces

We consider the contact of two elastic bodies with rough surfaces at the interface. The size of the micro-peaks and valleys is very small compared with the macrosize of the bodies' domains. This makes the direct application of the FEM for the calculation of the contact problem prohibitively costly. A method is developed that allows deriving a macrocontact condition on the interface. The method involves the twoscale asymptotic homogenization procedure that takes into account the microgeometry of the interface layer and the stiffnesses of materials of both domains. The macrocontact condition can then be used in a FEM model for the contact problem on the macrolevel. The averaged contact stiffness obtained allows the replacement of the interface layer in the macromodel by the macrocontact condition.
Keywords: asymptotic homogenization, contact problems
(28 pages, 2004)

60. A. Scherrer, K.-H. Küfer, M. Monz, F. Alonso, T. Bortfeld

IMRT planning on adaptive volume structures – a significant advance of computational complexity

In intensity-modulated radiotherapy (IMRT) planning the oncologist faces the challenging task of finding a treatment plan that he considers to be an ideal compromise of the inherently contradictive goals of delivering a sufficiently high dose to the target while widely sparing critical structures. The search for this a priori unknown compromise typically requires the computation of several plans, i.e. the solution of several optimization problems. This accumulates to a high computa-

tional expense due to the large scale of these problems - a consequence of the discrete problem formulation. This paper presents the adaptive clustering method as a new algorithmic concept to overcome these difficulties. The computations are performed on an individually adapted structure of voxel clusters rather than on the original voxels leading to a decisively reduced computational complexity as numerical examples on real clinical data demonstrate. In contrast to many other similar concepts, the typical trade-off between a reduction in computational complexity and a loss in exactness can be avoided: the adaptive clustering method produces the optimum of the original problem. This flexible method can be applied to both single- and multi-criteria optimization methods based on most of the convex evaluation functions used in practice.
Keywords: Intensity-modulated radiation therapy (IMRT), inverse treatment planning, adaptive volume structures, hierarchical clustering, local refinement, adaptive clustering, convex programming, mesh generation, multi-grid methods
(24 pages, 2004)

61. D. Kehrwald

Parallel lattice Boltzmann simulation of complex flows

After a short introduction to the basic ideas of lattice Boltzmann methods and a brief description of a modern parallel computer, it is shown how lattice Boltzmann schemes are successfully applied for simulating fluid flow in microstructures and calculating material properties of porous media. It is explained how lattice Boltzmann schemes compute the gradient of the velocity field without numerical differentiation. This feature is then utilised for the simulation of pseudo-plastic fluids, and numerical results are presented for a simple benchmark problem as well as for the simulation of liquid composite moulding.
Keywords: Lattice Boltzmann methods, parallel computing, microstructure simulation, virtual material design, pseudo-plastic fluids, liquid composite moulding
(12 pages, 2004)

62. O. Iliev, J. Linn, M. Moog, D. Niedziela, V. Starikovicius

On the Performance of Certain Iterative Solvers for Coupled Systems Arising in Discretization of Non-Newtonian Flow Equations

Iterative solution of large scale systems arising after discretization and linearization of the unsteady non-Newtonian Navier–Stokes equations is studied. cross WLF model is used to account for the non-Newtonian behavior of the fluid. Finite volume method is used to discretize the governing system of PDEs. Viscosity is treated explicitely (e.g., it is taken from the previous time step), while other terms are treated implicitly. Different preconditioners (block–diagonal, block–triangular, relaxed incomplete LU factorization, etc.) are used in conjunction with advanced iterative methods, namely, BiCGStab, CGS, GMRES. The action of the preconditioner in fact requires inverting different blocks. For this purpose, in addition to preconditioned BiCGStab, CGS, GMRES, we use also algebraic multigrid method (AMG). The performance of the iterative solvers is studied with respect to the number of unknowns, characteristic velocity in the basic flow, time step, deviation from Newtonian behavior, etc. Results from numerical experiments are presented and discussed.
Keywords: Performance of iterative solvers, Preconditioners, Non-Newtonian flow
(17 pages, 2004)

63. R. Ciegis, O. Iliev, S. Rief, K. Steiner

On Modelling and Simulation of Different Regimes for Liquid Polymer Moulding

In this paper we consider numerical algorithms for solving a system of nonlinear PDEs arising in modeling of liquid polymer injection. We investigate the particular case when a porous preform is located within the mould, so that the liquid polymer flows through a porous medium during the filling stage. The nonlinearity of the governing system of PDEs is due to the non-Newtonian behavior of the polymer, as well as due to the moving free boundary. The latter is related to the penetration front and a Stefan type problem is formulated to account for it. A finite-volume method is used to approximate the given differential problem. Results of numerical experiments are presented.
We also solve an inverse problem and present algorithms for the determination of the absolute preform permeability coefficient in the case when the velocity of the penetration front is known from measurements. In both cases (direct and inverse problems) we emphasize on the specifics related to the non-Newtonian behavior of the polymer. For completeness, we discuss also the Newtonian case. Results of some experimental measurements are presented and discussed.
Keywords: Liquid Polymer Moulding, Modelling, Simulation, Infiltration, Front Propagation, non-Newtonian flow in porous media
(43 pages, 2004)

Status quo: April 2004